

All-in-one Superparamagnetic and SERS-active Niosomes for Dual-targeted in Vitro Detection of Breast Cancer Cells

Viktor Maurer

Technische Universität Braunschweig: Technische Universität Braunschweig

Ajmal Zarinwall

TU Braunschweig: Technische Universität Braunschweig

Zunhao Wang

Physikalisch-Technische Bundesanstalt

Stefan Wundrack

Physikalisch-Technische Bundesanstalt

Nicole Wundrack

Otto-von-Guericke-University Magdeburg: Otto von Guericke Universität Magdeburg

Didem Ag Selesi

Technische Universität Braunschweig: Technische Universität Braunschweig

Vivien Helm

Technische Universität Braunschweig: Technische Universität Braunschweig

Daniil Otenko

Technische Universität Braunschweig: Technische Universität Braunschweig

Claudia Frank

Physikalisch-Technische Bundesanstalt

Fred Schaper

Otto-von-Guericke-University Magdeburg: Otto von Guericke Universität Magdeburg

Rainer Stosch

Physikalisch-Technische Bundesanstalt

Georg Garnweitner (✉ g.garnweitner@tu-bs.de)

Technische Universität Braunschweig Fakultät für Maschinenbau: Technische Universität Braunschweig
Fakultät für Maschinenbau <https://orcid.org/0000-0002-7499-4947>

Research Article

Keywords: hybrid nanoparticles, SERS, niosomes, diagnosis

Posted Date: December 14th, 2021

DOI: <https://doi.org/10.21203/rs.3.rs-1103948/v1>

License:  This work is licensed under a Creative Commons Attribution 4.0 International License.

[Read Full License](#)

Abstract

Background

In vitro and in vivo biosensing through surface-enhanced Raman scattering often suffer from signal contamination diminishing both the limit of detection and quantification. However, overcoming the lack of specificity requires excessive nanoparticle concentrations, which may lead to adverse side effects if applied to patients.

Results

We propose encapsulation of iron oxide (Fe_xO_y) and gold (Au) nanoparticles (NPs) into the bilayer structure of transferrin-modified niosomes. This approach enables achieving greatly enhanced and contamination-free SERS-signals in vitro as well as a dual-targeting functionality towards MCF-7 breast cancer cells. An in-depth characterization of Fe_xO_y NPs- and AuNPs-loaded niosomes ($\text{AuNPs}/\text{Fe}_x\text{O}_y\text{NPs}/\text{NIO}$) after magnetic downstream processing reveals defined hybrid niosome structures, which show a long-term SERS-signal stability in various media such as MCF-7 cell culture medium. In vitro 2D-SERS imaging unveil a successful incorporation of a non-toxic dose of hybrid NPs into MCF-7 cells, which leads to strong and almost contamination-free SERS-signals. The measured signal-to-noise ratio of the in vitro signal exceeds the values required by DIN 32645 for the successful validation of a detection method.

Conclusions

The hybrid niosomes can be considered a promising and efficient agent for the establishment and commercialization of a highly sensitive detection kit for monitoring cancerous tissue.

Introduction

Nowadays, the survival rate for diseases such as breast cancer is significantly increased in the early stages of diagnosis and can be further improved by the availability of highly sensitive detection methods that allow an accurate monitoring of the disease progression [1–3]. Although widespread screening programs can crucially reduce the mortality rate, the current limitations in sensitivity and specificity of the existing imaging techniques explain an insufficient detection of smaller cancerous tissues, which results in complications and the need for invasive therapeutic procedures (e.g. resection of the breast) as well as disease recurrence [4–7]. Consequently, there is an increasingly pressing demand for accurate and cost-efficient cancer detection methods.

An emerging technique, the so called surface-enhanced Raman spectroscopy (SERS), provides outstandingly specific and sensitive detection of analytes such as biomarkers, cells and tissues, with accuracy reaching single-molecule level [8–11]. Using specially designed analytical nanoparticles (NPs) as SERS-tags, the target moieties can be selectively bound by the NPs and detected indirectly through the

Raman signature of a Raman reporter molecule [12–14]. In contrast to the established bioimaging methods, SERS offers multiple advantages such as exceptionally high sensitivity, intrinsic molecular fingerprint information, resistance to photobleaching and –degradation as well as a non-invasive long-term multiplex monitoring within various applications [11, 15–18]. Despite proving its efficacy in several breast cancer-related in vitro, in-vivo and ex-vivo studies [19–22], the clinical establishment of SERS still remains challenging due to several drawbacks: i) the slow uptake rate of bare SERS-tags, ii) uncertain biocompatibility, iii) interfering species (e.g. a protein corona) adsorbing onto the metallic surface after in vitro/in vivo administration. These drawbacks increase the noise signal and induce signal contamination [23–27]. Unspecific absorption of biomolecules onto NPs in biological environments may lead to unforeseen physicochemical NP interactions followed by agglomeration and major signal fluctuations [28–30]. This results in a deteriorated detection limit which is detrimental for the successful validation of a diagnostic procedure according to the German standard method DIN 32645 and other international guidelines, thus hindering the establishment of a reliable detection method [31].

To overcome these obstacles, an encapsulation of the prepared SERS-tags becomes progressively common. By using different inorganic (e.g. silica [32, 33]) or organic (mostly liposomes/lipids [34–36], polyethylene glycole (PEG) [37, 38]) substances, single or multiple NPs can be incorporated in a shell of the respective substance. Especially an encapsulation of multiple functionalized plasmonic NPs into one carrier NP improves the biocompatibility, impedes the leaching of Raman-active molecules, reduces undesired NP-NP interactions and prevents signal contamination [18, 35, 39]. In addition, a shell-based spatial confinement of several NPs enhances the generation of plasmonic hot spots at interparticle gaps which yields in a drastic enhancement of SERS signal intensity [40–42]. Even though plasmonic NPs-loaded liposomes are continuously being developed for implementation in biomedical research [43–45], prevailing drawbacks still have to be addressed for a successful applicability. Most of the encapsulation procedures lack efficiency and require multiple post-synthetic purification steps to separate bare metallic NPs from the hybrid NPs, often leading to low yields and hence insufficient SERS signal intensities [46, 47]. Moreover, the low physical and chemical stability of liposomes can result in a degradation of the structural integrity and leakage of the liposome structure throughout encapsulation and application [45, 48, 49]. Therefore, a novel method to assemble stable hybrids of encapsulated metal NPs is eminently needed.

To circumvent these case problems, another type of organic NPs, the so-called niosomes, can be utilized, which are also capable of entrapping optically active NPs to detect and visualize cancer [51]. Niosomes are vesicular carriers made of non-ionic surfactants forming a bilayer structure that allows the simultaneous encapsulation of hydrophilic and lipophilic compounds [52–54]. Due to the surfactants, niosomes have a chemically and physically stable structure which enables long storage times [55]. Additionally, their non-ionic nature makes them highly biocompatible and biodegradable as well as cost-efficient [56, 57]. The surface of niosomes can easily be modified with various biomarkers to address a targeting functionality [54]. These outstanding properties entitle niosomes a particular promising material for various future applications, with clinical trials already indicating a successful nanocarrier capability [55–57].

Herein, we present a concurrent encapsulation of 5-thio-2-nitrobenzoic acid (TNB)-functionalized gold nanoparticles (AuNPs) and superparamagnetic iron-oxide nanoparticles (Fe_xO_y NPs) to accomplish the synthesis of the first niosomes with magnetic and SERS-active properties (**Figure 1**). The hydrophilic AuNPs and hydrophobic Fe_xO_y NPs were synthesized, functionalized and characterized as described in previous publications [62, 63]. PEG-maleimide-functionalized niosomes (NIO) and simultaneous encapsulation of the inorganic NPs were prepared using the thin-film hydration method similar to a recently published work [51], followed by a magnetic purification procedure. Finally, the niosome surface was decorated with transferrin (Tf) to augment the uptake by malignant breast cancer cells via Tf-receptor-mediated endocytosis [51, 64, 65]. Throughout the hybrid niosome assembly, we investigated mainly two parameters to further enhance the resulting SERS-signal intensity: the addition of an ionic substance (HCl) to the AuNP solution before encapsulation and the overall AuNP mass fraction impact. The successful hybrid niosome (AuNPs/ Fe_xO_y NPs/NIO/Tf) preparation was verified by investigating various particle properties using several methods such as i) dynamic light scattering (DLS), ii) SERS, iii) transmission electron microscopy (TEM), iv) UV/Vis Spectroscopy and iv) Zeta potential measurements. Moreover, by suspending the hybrid niosomes in different (complex biological) media, the long-term SERS-signal integrity and occurrence of possible signal contaminations was analysed over a period of 46 days. Ultimately, after verifying the biocompatibility within in vitro cytotoxicity studies, the hybrid niosomes were used for a 2D-SERS mapping of malignant MCF-7 breast cancer cells, hereby investigating the SERS-activity and signal integrity of the hybrid niosomes as well as confirming a successful detection according to national and international guidelines, such as the German standard method DIN 32645. Consequently, the hybrid niosomes revealed highly advantageous properties, combining excellent chemical stability, enhanced targeting functionality and remarkable SERS signal intensities, leading to great potential of the AuNPs/ Fe_xO_y NPs/NIO/Tf as a sensitive SERS-based cancer detection platform technology.

Results And Discussion

3.1 Raman properties of the AuNPs

In general, a reproducible application of SERS can only be realised by plasmonic nanoparticles with homogeneous particle properties. Therefore, an in-depth characterization of the AuNP plasmonic properties is essential. To investigate the influence of ripening time and core colloid size on the SERS activity, the synthesis of four final AuNP solutions was carried out using two core colloids with a size difference of 4.5 nm (**Figure S1 a**) after specific core colloid ripening times (10 and 42 days as well as 1 and 51 days, respectively). Representative TEM images of the four synthesized AuNP samples confirm equally sized particles of approx. 38-40 nm with no morphological variances (**Figure 2 a**).

All TNB-functionalized AuNPs were measured analogously via SERS by adding HCl as stated in section 4 (characterization methods) to characterize the Raman enhancing ability. Figure 2 b) illustrates a typical Raman spectrum of the TNB-functionalized AuNPs with the characteristic Raman peaks at 852 cm^{-1}

(nitro scissoring vibration), 1067 cm^{-1} (succinimidyl stretch overlapping with aromatic ring modes), 1341 cm^{-1} (symmetric stretch of the nitro group) and 1559 cm^{-1} (aromatic ring stretching modes) [66]. For further SERS intensity comparisons between the obtained TNB spectra, the intensity of the dominating nitro group stretch signal mode at 1341 cm^{-1} was used and referred to as the “maximum Raman intensity”.

After different final colloid ripening times (up to 120 days), SERS-spectra were measured (Figure 2 c). For all AuNPs, a longer final colloid ripening time results in a higher maximum Raman intensity. By comparing the AuNPs synthesized from the core colloids with the same size but different core colloid ripening times, a superior maximum Raman intensity after identical final colloid ripening times as a consequence of a longer core colloid ripening time becomes obvious. Apart from the ripening times, the core colloid particle size shows strong impact on the Raman intensity: AuNPs with a similar core colloid ripening time (AuNP 1.1 and AuNP 2.1, AuNP 1.2 and AuNP 2.2) still differ in their maximum Raman intensity at identical final colloid ripening times. The fact that larger core colloids lead to increased Raman intensities can be attributed to the high crystallinity of the core particles, which predominantly contribute to the Raman enhancing effect in contrast to the partly amorphous AuNP shell [62]. Since the limit of detection (LOD) and limit of quantification (LOQ) crucially depend on the signal-to-noise ratio, these results emphasise that larger core colloids with longer core and final colloid ripening times are essential to achieve higher Raman intensities and consequently to gain more sensitivity. For the following experiments, AuNPs which reached a maximum Raman intensity of approx. 2200 s^{-1} were used.

3.2 Synthesis of magnetic and SERS-active niosomes

The concurrent encapsulation of the TNB-functionalized AuNPs (in the presence or absence of HCl while AuNP preparation) and Fe_xO_y NPs was performed following the procedures shown in Figure 1. To verify the Raman enhancing ability of the encapsulated AuNPs as well as the successful magnetic separation process, SERS-spectra were recorded before magnetic purification (red spectra) and after removing the supernatant (yellow spectra) from the magnetically separated product (blue spectra) (**Figure 3**).

For the hybrid niosome samples, a distinct Raman intensity after the magnetic separation procedure was measured, indicating the presence of TNB-functionalized AuNPs. Comparing the sample with the respective negative control (blue spectra Figure 1 a with b), the difference

of 30.1 s^{-1} ($37.0\text{ s}^{-1} - 6.4\text{ s}^{-1}$) implies successfully encapsulated and magnetically separated TNB-functionalized AuNPs. With previously included HCl, a higher intensity difference of 87.1 s^{-1} ($95.0\text{ s}^{-1} - 7.9\text{ s}^{-1}$) for the hybrid niosome sample and negative control (blue spectra Figure 1 c with d) was obtained. In contrast to the samples without HCl, the substantially higher Raman intensity of the HCl-treated AuNP sample implicates the successful encapsulation of more AuNPs due to the acid-induced reduction of the AuNP surface charge, hence lowering the repulsion forces and distances from each other throughout the encapsulation process.

Apart from the preceding addition of an ionic substance (e.g. HCl), the Raman intensity can be increased by using higher AuNP amounts in the encapsulation procedure (**Figure 4 a**). While AuNP amounts below 20 μg result in almost negligible Raman intensities, raised amounts (40 μg , 50 μg and 80 μg) lead to a sharp intensity increase. This disproportionate Raman intensity surge can be attributed to an enlarged amount of encapsulated AuNPs per niosome and thus a larger number of generated interparticle plasmonic hotspots generated. If **Figure 4: Measured maximum Raman intensities of a) hybrid niosomes after addition of different AuNP mass fractions and b) hybrid niosomes and negative controls (with a utilized AuNP mass of both 50 μg and 80 μg) in dependence of a previous HCl addition.**

the amount of AuNPs is further incremented (for example to 200 μg), only a smaller rise in signal intensity was measured, suggesting a saturation of niosomes with encapsulated gold nanoparticles thus indicating that the average number of AuNP per niosome can hardly be increased. Comparing 50 μg and 80 μg hybrid niosomes samples with added HCl (Figure 4 b), the 80 μg sample shows a maximum Raman intensity either due to an amplified amount of encapsulated AuNPs, lower repulsion forces between incorporated AuNPs or both. When using 80 μg AuNPs instead of 50 μg , the difference between the mean intensities of the respective AuNP(HCl)/ $\text{Fe}_x\text{O}_y\text{NPs/NIO}$ to the respective negative control (MIX AuNP(HCl) with $\text{Fe}_x\text{O}_y\text{/NIO}$) grows significantly. This implies that in contrast to the lower amount, the addition of 80 μg AuNPs before encapsulation process leads to an amplified maximum Raman intensity of the resulting hybrid niosomes, whereas the amount of AuNPs, that remains in the solution after magnetic separation and still generates low Raman signals, is almost identical. Furthermore, even after removing a significant amount of AuNPs in the magnetic separation procedure, the AuNP (80 μg , HCl)/ $\text{Fe}_x\text{O}_y\text{NPs/NIO}$ surpasses the maximum Raman intensity of a plain 80 μg AuNP dispersion, indicating a successful SERS-active niosome synthesis. Since the maximum Raman intensity of hybrid niosome samples with less than 80 μg AuNPs is quite low and the use of AuNP amounts above 80 μg often resulted in particle agglomeration (data not shown), for all further experiments, unless otherwise stated, an amount of 80 μg AuNPs with previously added HCl was utilized for the hybrid niosomes preparation (in the following simply referred to as AuNPs/ $\text{Fe}_x\text{O}_y\text{NPs/NIO}$).

Repeated measurements of the hybrid niosomes SERS-activity during a period of 46 days reveal hardly any SERS-signal intensity fluctuations over the first 11 days (**Figure S1 b**). The increase in signal intensity by approx. 37 % within the following 35 days is probably due to a continuous agglomeration of the entrapped AuNPs. Stable SERS-activity is a good indication for a long-term stability of the hybrid niosome suspension.

Additionally, TEM images were recorded to display the successful encapsulation of the inorganic NPs (**Figure 5**). A representative TEM image of TNB-functionalized AuNPs that exhibit a strong contrast to the background can be seen in Figure 5 a). If only AuNPs are encapsulated into niosomes, the edges of the AuNPs are surrounded by a greyish layer, which can be attributed to the disintegrated organic niosome shell (Figure 5 b). An encapsulation of $\text{Fe}_x\text{O}_y\text{NPs}$ in niosomes leads to the occurrence of smaller and less contrasting $\text{Fe}_x\text{O}_y\text{NP}$ clusters with a diameter of around 100 nm that can be related to niosomes (Figure 5

c). After co-encapsulation of AuNPs and $\text{Fe}_x\text{O}_y\text{NPs}$, the formation of defined AuNPs/ $\text{Fe}_x\text{O}_y\text{NPs}$ /NIO hybrid NPs can be clearly recognized in the TEM images (Figure 5 d - i). Next to the bigger high-contrast AuNPs, smaller low-contrast $\text{Fe}_x\text{O}_y\text{NPs}$ are located, with both NP types being surrounded by an organic shell structure, thereby forming the hybrid niosome. Most frequently, four AuNPs were found to be incorporated per niosome (Figure 5 d - f) whereas the observed number varies between one and up to 15 AuNPs (Figure 5 g - i). It should be noted that the size of the hybrid niosomes in the pictures is in the range of 150-250 nm, which can be attributed to the destruction of the spherical 3D structure due to sample drying and the electron beam focus, leading to the formation of a planar and therefore larger quasi-2D layer.

To get a deeper insight into the SERS activity of AuNPs/ $\text{Fe}_x\text{O}_y\text{NPs}$ /NIO, the resulting electromagnetic field (E-field) enhancement, which is created by the electromagnetic radiation of metallic NPs, was calculated using finite-difference time-domain simulations (FDTD)

Figure 6: a) Schematic representation of AuNPs/ $\text{Fe}_x\text{O}_y\text{NPs}$ /NIO utilized for the FDTD simulations; b) calculated maximum E-field enhancement on the AuNP surface for AuNPs/ $\text{Fe}_x\text{O}_y\text{NPs}$ /NIO and AuNPs/NIO with variant interparticle gap; FDTD simulated E-field enhancement of AuNPs/ $\text{Fe}_x\text{O}_y\text{NPs}$ /NIO with a AuNP (encircled in gold) gap distance of 4 nm c), 10 nm d) and the AuNPs/ $\text{Fe}_x\text{O}_y\text{NPs}$ /NIO from the Figure 5 e) TEM image.

simulations. For the AuNPs/ $\text{Fe}_x\text{O}_y\text{NPs}$ /NIO, TNB as the Raman-active compound is immobilized onto the AuNPs, which are encapsulated in a water-filled, spherical niosome bilayer (Figure 6 a). The FDTD simulation demonstrated that the $\text{Fe}_x\text{O}_y\text{NPs}$ -containing niosome layer does not significantly influence the resulting E-field on amplification the surface of the AuNPs at various distances (Figure 6 b). Furthermore, the highest enhancement of the E-field on the inside of the niosome layer is several orders of magnitude lower than between two AuNP surfaces, even at a maximum interparticle distance (approx. 10 nm for two 40 nm sized AuNPs inside a 90 nm niosome core) (Figure 6 c and d). This confirms that, as already demonstrated in Figure 3 experimentally, the measured SERS-spectra of the AuNPs/ $\text{Fe}_x\text{O}_y\text{NPs}$ /NIO are almost exclusively composed of the specific vibrations of the TNB and do not exhibit any structural artefacts of the $\text{Fe}_x\text{O}_y\text{NPs}$ /NIO. Simulating the E-field enhancement of the AuNPs/ $\text{Fe}_x\text{O}_y\text{NPs}$ /NIO illustrated in the TEM-image of Figure 5 d, a congruent result was obtained (Figure 6 e) as well as for AuNPs/NIO in Figure 5 b (Figure S3).

Recorded UV/Vis-spectra illustrate an overall reduction in extinction (especially the AuNP-specific maximum) for the hybrid niosomes and negative controls after magnetic separation, indicating a lower concentration of NPs in the resulting suspensions (Figure 7 a). **Figure 7: Measured UV/Vis spectra a) before and after magnetic purification obtained from hybrid niosomes and negative controls and b) hybrid niosomes with different AuNPs mass fractions as well as with and without previously added HCl.**

Since the majority of the AuNPs in the negative control sample is removed after magnetic purification, a AuNP-specific maximum is hardly visible. The large optical density (OD) discrepancy of the magnetically purified dispersions can thus be attributed to the successful AuNP encapsulation and hence raised mass fraction in the solution. Although the AuNPs/Fe_xO_yNPs/NIO sample after magnetic separation contain a lower AuNP amount than the supernatant sample (**Figure S4** a and b), Figure 3 showed that the exhibited SERS-intensity after magnetic separation is several times higher than the resulting SERS-intensity of the supernatant, which is a clear evidence for encapsulation and thereby induced SERS-activity.

Furthermore, the spectra of AuNPs/Fe_xO_yNPs/NIO samples with different AuNPs mass fractions were compared (Figure 7 b). Regardless of a previous HCl addition, a higher OD and thus an increased number of encapsulated AuNPs is obtained after induction of a higher AuNP mass fraction within the encapsulation procedure. This relation is in good agreement with the SERS results displayed in Figure 4. A further analogy to the results of the SERS measurements becomes comprehensible when comparing UV/Vis spectra of the same AuNP mass: adding HCl before the encapsulation process also leads to an elevated OD suggesting a more efficient encapsulation of AuNPs. Moreover, compared to the samples without included HCl, the spectra **Figure 8: a) DLS measurements and b) Zeta potentials of the hybrid niosomes and negative control.**

of the HCl-treated AuNP samples reveal a more steadily decreasing curve profile after the maximum at approx. 526 nm, which becomes clearer when comparing the first derivative of the curves: after the minimum at around 560 nm, the slope of the samples without added HCl increases faster than the slope of the samples with HCl-treated AuNP, which even display smaller minima at approx. 730 nm (Figure S4 c). This can be attributed to the HCl-induced proximity among AuNPs within the hybrid structure and the resulting coupling of their surface plasmon resonance [67, 68].

DLS measurements confirm that the average particle size of the hybrid niosomes and negative control after magnetic separation is approximately 120 nm which predominantly indicates the presence of niosomes (**Figure 8** a). This hydrodynamic diameter is in the size range of bare Fe_xO_yNPs/NIO, which is expected to ensure a flawless uptake by cancer cells via receptor-mediated endocytosis [69–71].

Furthermore, it is shown that the Zeta potential of the AuNPs/Fe_xO_yNPs/NIO and the negative control are almost equal after magnetic separation and correspond to the value of Fe_xO_yNPs/NIO, thus proving a successful magnetic separation procedure (**Figure 8** b). Moreover, the final Zeta potential of -35 mV indicates an electrostatically well-stabilized suspension. The Zeta potential of the supernatants resemble the AuNP-specific Zeta potential due to the abundance of free AuNPs (**Figure S5** a and b).

3.3 Administration of hybrid niosomes to complex media

After the successful synthesis, magnetic purification and characterization of the AuNPs/Fe_xO_yNPs/NIO, an investigation of the niosomal shielding effect on the SERS-signal integrity against external influences (e.g. high osmotic pressure, biological molecules, acidic environment etc.) that usually affect NPs after

administration in organisms was realized. For this purpose, three different media were prepared: phosphate-buffered saline (PBS), a saturated

bovine serum albumin (BSA) suspension and the cell culture medium (CCM) used to cultivate MCF-7 breast cancer cells. After the addition of the respective medium, there is initially a slight reduction in the SERS signal intensity ("0 days"), which is mainly due to the dilution of the respective sample. If PBS is added to plain TNB-functionalized AuNPs, a strong increase in the SERS-signal intensity is initially recorded due to a reduction of the repulsive forces between the AuNPs, thus resulting in an exalted generation of interparticle SERS-hotspots (**Figure 9 a**). This is followed by a rapid decrease within the first hours, which finally leads to a complete and persistent loss of SERS-signal due to particle agglomeration. The hybrid niosomes, on the other hand, show no major fluctuations as a result of the niosomal shielding, with a decrease in signal intensity of approximately 35% only after an extended storage. This is probably caused by a partial loss of the structural integrity of some niosomes due to the high osmotic pressure of the PBS suspension. Nevertheless, qualitative identification of the symmetrical stretching vibrations of the nitro group is still clearly possible even after 46 days (Figure 9 b). After addition of the BSA solution to plain AuNPs, a steady decrease in signal intensity was observed, followed by a stable signal intensity until the 46th day (Figure 9 a). In contrast, the signal fluctuations of the hybrid niosomes are again negligible throughout the entire measurement period, and an enhanced SERS signal intensity with only a small proportion of signal contamination is seen in the spectrum at longer storage times (Figure 9 c), mainly attributed to the high concentration and consequently increased Raman-scattering of BSA. The change in the signal intensity of the hybrid niosomes in CCM and the underlying causes are rather analogous to the case of PBS due to a similarly high osmotic pressure. The SERS signal intensity of the plain AuNPs in CCM decreases sharply within the first days and remains below the detection limit for the further measurements. The reason for this is a strong signal contamination by the components of CCM, which are adsorbed onto the AuNP surface and thus do not allow a clear identification of the symmetrical stretching oscillation of the nitro group (Figure 9 d).

To investigate possible signal variations due to an acidic environment (as present in most cancer cells), HCl (1 M, 4 μ L) was added post-synthetically to hybrid niosomes and negative control dispersions (**Figure S2 a**). In contrast to the plain AuNP solution, no significant Raman intensity changes occurred in any of the niosome-containing samples, indicating the prevention of different interparticle hotspot generation. Furthermore, encapsulated AuNPs are shielded by the niosomes against the surrounding acid, whereas the niosomes in the MIX negative control sample may sterically prevent a spatial approximation of the AuNPs. Further pH measurements confirm that these results are not based on a pH-buffering ability of the niosomes since the acid addition results in a pH decrease to 2.0-2.2 for all samples (Figure S2 b). Moreover, the neutral pH-values of the AuNPs(HCl)/Fe_xO_yNPs/NIO samples before applying the acid prove that the initially included HCl has been removed in the dialysis step, thus indicating the possibility of further in vitro experiments without acid-based side effects.

These results suggest that the niosomes act as a protective layer against a wide range of different molecules and pH-shifts found in biological environments, thus serve to maintaining the SERS-activity

over a long storage period. In particular, the results in CCM show that after administration of the particles in vitro, no signal contamination by the cultivation medium itself and therefore no influence of the medium on cell imaging can be expected.

3.4 In vitro experiments

Since intracellular SERS detection vitally depends on the efficient internalization of the SERS nanoprobes, it is highly important to develop methods that can effectively deliver the SERS-active NPs into the cell. Considering that a disordered iron metabolism is a hallmark of cancer cells, the Tf-receptor is commonly used as a prominent marker of cancer cells and also identified as a therapeutic target [72]. Remarkably, Tf-receptor 1 (CD71) [73, 74], but also other iron-regulating and -regulated proteins such as transcription factors [75] are overexpressed in human breast cancer cells. Therefore, apart from a successful iron-oxide based magnetic targeting with an external magnetic field [63, 76], a second, cell-specific targeting functionality was necessary. As the niosomes are to be used to label breast cancer cells, the Tf-receptor system is a preferable route for internalization of niosomes. Thus, Tf was coupled to the maleimide groups of the hybrid niosomes. The successful Tf-functionalization of the hybrid niosomes was investigated using Zeta potential measurements, which clearly showed a decrease in the absolute value of the Zeta potential due to the coupling of positively charged Tf (**Figure S6**) similar to the results reported in other works [51, 77].

Since the synthesized hybrid niosomes will be primarily used for the detection of living breast cancer cells, particularly uncontrolled necrotic signal cascades should be avoided. Hence, **Figure 10: Viability of MCF-7 cells after in vitro administration of hybrid niosomes with or without Tf-functionalization and incubation under influence of an external magnetic field.**

cytotoxicity studies were carried out using MCF-7 breast cancer cells (**Figure 10**). From the results of our experiments, we conclude that a hybrid niosomes volume of at least 14 μL per 10k MCF-7 cells leads to no significant reduction in viability and therefore can be assumed as a safe volume for in vitro administration. However, for hybrid niosome volumes larger than 14 μL , surface modification with Tf leads to slightly reduced viability. This interference can be attributed to an increased uptake of the functionalized hybrid niosomes due to a successful Tf-receptor-mediated endocytosis.

In vitro 2D SERS images clearly demonstrate that the dyadic targeting composed of a magnetic manipulation as well as Tf-based endocytosis resulted in the accumulation of AuNPs/ $\text{Fe}_x\text{O}_y\text{NPs}$ /NIO in MCF-7 cells after 24 hours of incubation (**Figure 11**). Strong localized TNB-signals were detected, possibly indicating an accumulation in specific cell compartments, as well as a non-specific accretion throughout the cytosol of the cell. The oscillation of the TNB nitro group in the in vitro SERS-spectra is located at approx. 1341 cm^{-1} as in the TNB-reference spectra. Apart from a minor background noise, no signal contamination can be detected, which indicates the structural integrity of the hybrid niosomes. The calculated

signal-to-noise ratios (SNR) are always clearly above the prescribed SNR minimum of 9.0 according to national and international guidelines, such as DIN 32645. In particular, the highest occurring SNR in the center of each region of interest is 3-4 times higher than the minimum requirement of 9, implicating a verified SNR as specified by the DIN standard. In vitro tests with HeLa cells also show an analogous outcome (**Figure S7**). These results prove the shielding effect of the niosomal protective layer and thus the great potential of the synthesized hybrid niosome system to be used for analytically labelling Tf-overexpressing cancer cells such as breast carcinoma cells.

Conclusion

In this study, we presented the first successful preparation and in vitro application of superparamagnetic and SERS-active niosomes. The synthesized AuNPs/Fe_xO_yNPs/NIO hybrid NPs exhibited SERS-signals that could be strongly enhanced by addition of HCl to the AuNPs before encapsulation or by using a higher overall AuNP mass fraction. The entrapped Fe_xO_yNPs enabled a magnetic purification procedure and magnetic targeting using an external magnetic field. An in-depth characterization revealed the formation of highly defined hybrid structures visible in a number of representative TEM images. Furthermore, the niosome shell induced the formation of interparticle hot spots and shielded the AuNPs from multiple influences such as high salt concentrations, protein coronas, and acidic environments, affirming an extraordinary colloidal SERS-signal stability. Functionalizing the surface with Tf led to an increased Zeta potential and a slightly decreased viability of hybrid niosome-containing MCF-7 cells at specific concentrations. These observations clearly point to an enhanced internalization efficacy of hybrid niosomes due to coupling Tf onto their surface. Using the dual targeting functionality by applying an external magnetic field after in vitro administration of Tf-modified hybrid niosomes, their cellular uptake by the MCF-7 cells was observed. The internalized hybrid niosomes exhibited eminent SERS-signal intensities with almost no signal contamination. All measured SNR ratios indicate a successful validation of the present detection procedure according to the German standard method DIN 32645. These results confirm the initial hypothesis of utilizing niosomes to produce chemically and physically stable hybrid NPs with superparamagnetic and SERS-active properties to achieve a SERS-based monitoring of breast cancer cells.

To validate SERS-based imaging and monitoring of tumorous tissues for ex vivo diagnosis or even for staining tumor cells in vivo using the presented hybrid niosomes, extensive and elaborate in vivo experiments are mandatory. Since we chose TNB as the Raman-active compound, the hybrid niosomes possess the inherent capability to establish a quantification principle using the isotope dilution (ID) technique, which has already been used in combination with SERS [78–80]. Therefore, apart from ex vivo quantification procedures to investigate biomarker concentrations in human fluids (blood, cerebrospinalfluid etc.), an in vivo ID-SERS approach could aim to establish a correlation between the isotope-based Raman-shift and 2D-SERS measurements to draw conclusions about the volume and shape of the tumor. In essence, the results from this study bear great potential to establish a novel and

highly sensitive imaging technique which allows monitoring and prospectively targeting of smallest cancerous breast tissues.

Materials And Methods

Chemicals and reagents

Benzyl ether (98 %), cholesterol (≥ 99 %), gold(III) chloride (99 %), 1,2-hexadecanediol (90 %), hydrochloric acid (HCl, 37 %), 4-(2-hydroxyethyl)-1-piperazineethanesulfonic acid (HEPES, ≥ 99.5 %), 2-iminothiolane hydrochloride (Traut's reagent, ≥ 98 %), insulin solution (human), iron(III) acetylacetonate ($\text{Fe}(\text{acac})_3$, ≥ 99 %), non-essential amino acid solution (100x), oleic acid (90 %), oleylamine (70 %), phosphate buffered saline (PBS, tablet form), phosphotungstic acid (99.99 %), polyethylene glycol 600 (PEG, techn. grade), sodium(L) ascorbate (≥ 98 %), sodium hydroxide (NaOH, ≥ 97 %), sodium pyruvate solution, sorbitan monostearate (Span60), transferrin (Tf, ≥ 98 %) and trypsin were obtained from Sigma-Aldrich Chemie GmbH (Taufkirchen, Germany). 1,2-distearoyl-sn-glycero-3-phosphoethanolamine-N-[maleimide(polyethyleneglycol)-2000] (DSPE-PEG(2000) maleimide) was provided by Avanti (Alabaster, USA). 5,5'-dithiobis-(2-nitrobenzoic acid) (DTNB, ≥ 99 %) was acquired from AppliChem GmbH (Darmstadt, Germany). Fetal calf serum (FCS) was ordered from Biochrom GmbH (Berlin, Germany). Absolute ethanol (EtOH, 99.5 %) was supplied by Fisher Scientific GmbH (Schwerte, Germany). Minimum essential medium (MEM) was purchased from Gibco life technologies (Carlsbad, USA). Ethylenediaminetetraacetic acid disodium salt dihydrate (EDTA, ≥ 99 %) and sodium citrate dihydrate (≥ 99.95 %) were ordered from Honeywell Fluka (Seelze, Germany). MCF-7 (breast adenocarcinoma) cell line was provided from German Collection of Microorganisms and Cell Cultures (DSMZ). All chemicals were used as received. Unless otherwise stated, ultrapure water was used. The HEPES buffer was prepared by dissolving HEPES powder (0.063 g) in ultrapure water (50 mL) and adjusting to a pH of 7.48-7.52 using a NaOH solution (0.1 mol/L). The PBS buffer (0.01 mol/L) for cell culture was obtained by dissolving one PBS tablet in ultrapure water (200 mL).

Synthesis of Fe_xO_y NPs

The solvothermal synthesis of the Fe_xO_y NPs and the particle properties were stated in our previous publication [63]. In summary, oleic acid (3 mmol) and oleylamine (3 mmol), $\text{Fe}(\text{acac})_3$ (1 mmol) and 1,2-hexadecanediol (5 mmol) were added to a flask containing benzyl ether (10 mL) and heated to 100 °C for 30 min. Under nitrogen atmosphere, the mixture was first refluxed at 200 °C and afterwards at 265 °C for 30 min each. The solution was cooled down to room temperature, followed by three washing steps with ethanol. After purification, the black precipitates were dispersed in chloroform. The notation Fe_xO_y is used in this report since the synthesized iron oxide NPs consist of both the magnetite Fe_3O_4 and maghemite $\gamma\text{-Fe}_2\text{O}_3$ phases.

Synthesis and TNB-functionalization of AuNPs

The synthesis procedure and a comprehensive characterization regarding the AuNP synthesis, TNB-functionalization and resulting particle properties (crystallinity, size, morphology etc.) was presented in our previous publication [62]. In short, the preparation of the core colloids was accomplished by refluxing a gold(III) chloride solution (206 mL) while heating at 100 °C for 30 min and for another 15 min after addition of 50 mL citric acid solution. The synthesis of the final colloids was carried out by appending a sodium-(L) ascorbate solution (233 mL) and a gold(III) chloride solution (233 mL) to a flask containing a core colloid solution (12 mL). Subsequently, after keeping the final solution at 30 °C for 1 h, the particles were purified via centrifuging and replacing the supernatant with HEPES buffer. By following this protocol, two different core colloids (AuNP 1 as well as AuNP 2) were synthesized. After specific ripening times, each core colloid was used to synthesize two final colloids (AuNP 1.1 and AuNP 1.2 as well as AuNP 2.1 and AuNP 2.2), respectively. The AuNP dispersions had a solid content of approx. 100 µg/mL (determined gravimetrically). The TNB-functionalization of AuNPs was performed by adding 10 µL of DTNB solution per 50 µg/mL of AuNP dispersion. After a 30 min incubation, the particles were purified twice by centrifugation and replacing the supernatant with HEPES buffer.

Hybrid niosome synthesis via niosomal incorporation of Fe_xO_yNPs and AuNPs

The synthesis of PEG-maleimide-functionalized niosomes was based on the thin-film hydration method according to the protocol stated by Ag Seleci et al. [58]. The incorporation of Fe_xO_yNPs to prepare Fe_xO_yNPs-loaded Niosomes (Fe_xO_yNPs/NIO) followed a slightly adapted procedure [63]. In short, Span60, cholesterol, and DSPE-PEG (2000) maleimide were dispersed in 1 mL chloroform (4.95:4.95:0.1 mmol/L). To this lipid mixture, 10 µL of Fe_xO_yNPs dispersed in chloroform (7.0 mg/mL) was added, followed by a rotary evaporation process for 2 h at 38 °C under decreased pressure (300 mbar). After successful formation of the lipid thin-film, 1 mL of TNB-functionalized AuNPs dispersed in water was added. In order to achieve lower repulsion forces between the AuNPs, HCl (2.5 µL) was put in some samples (referred to as AuNPs(HCl)). This was followed by sonication for 1 h at 65 °C. Then, utilizing a mini extruder set (Avanti Polar Lipids, USA), 20 extrusion cycles were performed, first using a 0.4 µm and then a 0.1 µm polycarbonate membrane to obtain the AuNPs/Fe_xO_yNPs/NIO hybrid NPs with an expected size of approx. 120 nm. To remove the excess HCl, a purification using a 12-14 kDa dialysis membrane was carried out for around 4 h. Finally, by attaching a 1.3 T permanent neodymium magnet to the samples for 16 h hours, the product containing the magnetically separated NPs (referred to as magn. sep.) and another sample with the remaining NPs in the supernatant (referred to as supernatant) was attained. For the preparation of a negative control consisting of a AuNP and Fe_xO_yNPs/NIO mixture (referred to as MIX AuNPs with Fe_xO_yNPs/NIO), ultrapure water (1 mL) was added to the thin-film containing flask to synthesize plain Fe_xO_yNPs/NIO, which was then sonicated and extruded as described before. Afterwards, the Fe_xO_yNPs/NIO solution (1 mL) was used to replace the decanted supernatant of precipitated TNB-functionalized AuNPs after the last purification step. Thereby, a mixture of AuNPs and Fe_xO_yNPs/NIO with the same AuNP mass content as the AuNPs/Fe_xO_yNPs/NIO sample was obtained, thus imitating a failed encapsulation process.

Finite-difference time domain simulations of E-field enhancement

The open-source software MEEP was utilized to perform two-dimensional finite-difference time-domain simulations (FDTD). Further explanation for the implemented FDTD algorithm and perfectly matched layers (PML) in MEEP can be found in the work of Oskooi et al. [81]. A series of Lorentzian functions fitted to the measurement of Johnson *et al.* acted as the dielectric function of gold. The refractive indices of niosomes as well as $\text{Fe}_x\text{O}_y\text{NPs}$ were set to 1.45 and 2.92, respectively, and water served as the background dielectric of the simulated structure [82, 83]. For the light source, a continuous plane wave was utilized with the wavelength set to 633 nm. One single Yee cell was sized as 0.1 nm \times 0.1 nm, whereas the remaining boundary conditions were PML. The E-field amplitude was output at all points in the area of interest. A calculation of the total E-field enhancement in one Yee cell was achieved by dividing the absolute square of the E-field amplitude with the squared amplitude of the incident E-field in the absence of the structure.

Preparation of Tf-conjugated hybrid niosomes

To prepare AuNPs/ $\text{Fe}_x\text{O}_y\text{NPs}$ /NIO/Tf, Traut's reagent (50 nmol) and Tf (10 nmol) were suspended in HEPES EDTA buffer (500 μL) at pH 8.5 (30 mM HEPES and 0.1 mM EDTA). The thiolation of Tf was completed after incubating for 2 h at room temperature. In addition, using a size exclusion chromatography (30 kDa, Sephadex G50, Cytiva), the thiolated Tf was washed with HEPES (pH 6.5) and concentrated to a final volume of 200 μL . This was followed by an immediate application of hybrid niosome suspension (750 μL). A subsequent incubation for 24 h at 4 $^\circ\text{C}$ resulted in the formation of a thioether linkage [84] and the binding of the Tf-specific thiol groups to the maleimide moieties of the niosome PEG chains.

SERS-measurements in different media

The SERS-signal fluctuations of the AuNPs/ $\text{Fe}_x\text{O}_y\text{NPs}$ /NIO/Tf hybrid NPs and a negative control (plain TNB-functionalized AuNPs with the same AuNP mass content) in PBS (0.04 M), BSA (40 mg/mL) and MCF-7 cell culture medium (volumetric mixing ratio of NPs suspension : added medium was 2.5:1 for all samples) were examined over a period of 46 days. For a sufficient comparability of the samples, the initial SERS signal intensities for both the hybrid niosomes and negative control were normalized.

In vitro experiments

For the in vitro experiments, the cells were seeded on TPP[®] 96-well plates (Sarstedt, for cytotoxicity studies) or Poly-L-Lysine-(Sigma-Aldrich, for 2D-SERS measurements) coated cover glasses and cultured for 24 h in DMEM (Thermo Fisher Scientific, Waltham, MA, USA) supplemented with 10% FCS (Thermo Fisher Scientific), streptomycin, and penicillin (each 100 μg per ml, Thermo Fisher Scientific) at 37 $^\circ\text{C}$ in a water saturated atmosphere containing 5% CO_2 . To assess the metabolic activity of MCF-7 cells after AuNPs/ $\text{Fe}_x\text{O}_y\text{NPs}$ /NIO/Tf administration, a CellTiter-Blue[®] cell viability assay was used to measure the reduction capacity of Resazurin (Promega Corp., Madison, WI, USA). 10^4 cells were seeded per well

with 200 μL added cultivation medium and cultivated for 48 h. Afterwards, the cells were exposed with different concentrations of bare or Tf-loaded hybrid niosomes, incubated for 15 min by attaching a 1.3 T permanent neodymium magnet to achieve a magnetic guidance and subsequently incubated for 24 h. After diluting the CellTiter-Blue® reagent 1:10 with supplement-free MEM medium, 200 μl of the suspension was added to each well and incubated at 37 °C and 5 % CO_2 for 4 h. A fluorescence spectrometer (GENios Microplate Reader, Tecan) was used to measure the fluorescence (530 nm excitation/590 nm emission). For the 2D-SERS measurements, the AuNPs/ Fe_xO_y NPs/NIO/Tf were added in a non-toxic concentration (14 μl). The cells were incubated under the influence of a magnetic field (1.3 T permanent neodymium magnet) for 15 minutes. Subsequently the cells were grown in a water saturated atmosphere containing 5% CO_2 for 24 h at 37 °C. Afterwards cells were fixed with 4 % paraformaldehyde (PFA, Carl Roth) at room temperature (21 °C) for 20 min and subsequently washed twice with PBS and mounted with Shandon Immu-Mount (9990402 EpreDia) for following SERS measurements.

Characterization methods

The DLS and Zeta potential measurements were accomplished using a Zetasizer Nano ZS from Malvern Instruments. To minimize fluorescence, the samples were diluted by a factor of 10^4 - 10^5 and subsequently measured with a 173° backscattering set-up thrice. Using the Zetasizer Nano software, the data was evaluated utilizing the intensity distributions to assess the hydrodynamic diameters. The Zeta potentials were attained using a capillary zeta cuvette (DTS1070C, Malvern Panalytical Ltd). The pH-values of samples were acquired with the pH-meter Seven Compact from Mettler Toledo. To obtain SERS spectra, a LabRAM Aramis Raman microscope equipped with a 600 grooves/mm holographic grating and a HeNe excitation laser (633 nm) in combination with the LabSpec 5 Software from Horiba was used. Each sample was irradiated with an exposure time of 200 · 1 s with a spot size around 550 nm. Prior to each acquisition, the spectral line position was calibrated according to the recommendations given in the ASTM guideline using the polystyrene ring breathing mode at 1001.4 cm^{-1} [85]. The SERS-spectra of plain AuNP solutions (in Section 3.1) were attained after adjusting their OD to 1 and adding HCl (4 μL , 1 M) to 250 μL of AuNP solution. For the 2D-SERS mappings, a 20x objective lens was used with an average image acquisition time of approx. 8 h. UV/Vis spectra were acquired using a LAMBDA 1050 dual-beam photometer from Perkin Elmer. The measurement was carried out in a Quartz Suprasil semi-micro cuvette (layer thickness 1.0 cm) from Hellma Analytics. TEM images were taken with a Tecnai G2 F20 TMP from FEI at 200 kV. For sample preparation, 20 μl of the solution were mixed with a staining solution (10 μl) containing 2 % aqueous phosphotungstic acid and applied onto a carbon film on a 3.05 mm woven copper net with 300 mesh from Plano GmbH. Particle sizes were determined by measuring 50 nanoparticles, using the ImageJ software (Version 1.42q).

Abbreviations

Bovine serum albumin (BSA), cell culture medium (CCM), 1,2-distearoyl-sn-glycero-3-phosphoethanolamine-N-[maleimide(polyethyleneglycol)-2000] (DSPE-PEG(2000) maleimide), 5,5'-dithiobis-(2-nitrobenzoic acid) (DTNB), dynamic light scattering (DLS), electromagnetic field (E-field), ethanol (EtOH), ethylenediaminetetraacetic acid disodium salt dihydrate (EDTA), fetal calf serum (FCS), finite-difference time-domain simulations (FDTD), german standard method 32645 (DIN 34645), gold (Au), iron oxide (Fe_xO_y), isotope dilution (ID), 4-(2-hydroxyethyl)-1-piperazineethanesulfonic acid (HEPES), limit of detection (LOD), limit of quantification (LOQ), MCF-7 (breast adenocarcinoma), minimum essential medium (MEM), nanoparticles (NPs), niosome (NIO), optical density (OD), perfectly matched layers (PML), phosphate-buffered saline (PBS), polyethylene glycol (PEG), signal-to-noise ratio (SNR), sorbitan monostearate (Span60), surface-enhanced Raman spectroscopy (SERS), 5-thio-2-nitrobenzoic acid (TNB), transferrin (Tf), Tf-receptor 1 (CD71), transmission electron microscopy (TEM).

Declarations

Acknowledgements

The authors thank the Laboratory of Nano and Quantum Engineering (LNQE) of the Leibniz University of Hanover for the TEM instrument.

Authors' contributions

VM designed and performed experiments, analyzed the results and wrote the manuscript. AZ, DA and CF performed further experiments and were responsible for additional data interpretation. ZW was responsible for the FDTD simulation. VM, VH, DO, SW and NW performed the experimental SERS trials. FS, RS and GG supervised the study and reviewed the manuscript. All authors approved the final manuscript.

Availability of data and materials

The datasets used and/or analyzed during the current study are available from the corresponding author upon reasonable request.

Funding

This research was partially funded by Niedersächsisches Ministerium für Wissenschaft und Kultur through the "Quantum- and Nano-Metrology (QUANOMET)" initiative (ZN3245) within the scope of the project NP-1.

Competing interests

The authors declare no competing financial interest.

Consent for publication

All authors agree to be published.

Ethics approval and consent to participate

Not applicable.

References

- [1] E. R. Myers, P. Moorman, J. M. Gierisch, L. J. Havrilesky, L. J. Grimm, S. Ghate, B. Davidson, R. C. Montgomery, M. J. Crowley, D. C. McCrory, A. Kendrick, G. D. Sanders. Benefits and Harms of Breast Cancer Screening: A Systematic Review. *JAMA*. 2015;314:1615-34.
- [2] W. H. Organization, WHO position paper on mammography screening. World Health Organization. Geneva. 2014.
- [3] R. Swaminathan, E. Lucas, R. Sankaranarayanan. Cancer survival in Africa, Asia, the Caribbean and Central America: database and attributes. *IARC Sci. Publ.* 2011:23-31.
- [4] J. Ferlay, M. Colombet, I. Soerjomataram, C. Mathers, D. M. Parkin, M. Piñeros, A. Znaor, F. Bray. Estimating the global cancer incidence and mortality in 2018: GLOBOCAN sources and methods. *Int. J. Cancer*. 2019;144:1941-53.
- [5] Early Breast Cancer Trialists' Collaborative Group (EBCTCG), R. Peto, C. Davies, J. Godwin, R. Gray, H. C. Pan, M. Clarke, D. Cutter, S. Darby, P. McGale, C. Taylor, Y. C. Wang, J. Bergh, A. Di Leo, K. Albain, S. Swain, M. Piccart, K. Pritchard. Comparisons between different polychemotherapy regimens for early breast cancer: meta-analyses of long-term outcome among 100 000 women in 123 randomised trials. *Lancet*. 2012;379:432-44.
- [6] Early Breast Cancer Trialists' Collaborative Group (EBCTCG). Aromatase inhibitors versus tamoxifen in early breast cancer: patient-level meta-analysis of the randomised trials. *Lancet*. 2015;386:1341-52.
- [7] H. Pan, R. Gray, J. Braybrooke, C. Davies, C. Taylor, P. McGale, R. Peto, K. I. Pritchard, J. Bergh, M. Dowsett, D. F. Hayes. 20-Year Risks of Breast-Cancer Recurrence after Stopping Endocrine Therapy at 5 Years. *N. Engl. J. Med.* 2017;377:1836-46.
- [8] K. Kneipp, H. Kneipp, I. Itzkan, R. R. Dasari, M. S. Feld. Ultrasensitive chemical analysis by Raman spectroscopy. *Chem. Rev.* 1999;99:2957-76.
- [9] J. Kneipp, H. Kneipp, K. Kneipp. SERS-a single-molecule and nanoscale tool for bioanalytics. *Chem. Soc. Rev.* 2008;37:1052-60.
- [10] J. N. Anker, W. P. Hall, O. Lyandres, N. C. Shah, J. Zhao, R. P. van Duyne. Biosensing with plasmonic nanosensors. *Nat. Mater.* 2008;7:442-53.

- [11] S. Laing, K. Gracie, K. Faulds. Multiplex in vitro detection using SERS. *Chem. Soc. Rev.* 2016;45:1901-18.
- [12] S. L. Kleinman, R. R. Frontiera, A.-I. Henry, J. A. Dieringer, R. P. van Duyne. Creating, characterizing, and controlling chemistry with SERS hot spots. *Phys. Chem. Chem. Phys.* 2013;15:21-36.
- [13] L. Fabris. SERS Tags: The Next Promising Tool for Personalized Cancer Detection? *ChemNanoMat.* 2016;2:249-58.
- [14] E. Lenzi, D. Jimenez de Aberasturi, L. M. Liz-Marzán. Surface-Enhanced Raman Scattering Tags for Three-Dimensional Bioimaging and Biomarker Detection. *ACS Sens.* 2019;4:1126-37.
- [15] G. Bodelón, V. Montes-García, C. Fernández-López, I. Pastoriza-Santos, J. Pérez-Juste, L. M. Liz-Marzán. Au@pNIPAM SERS Tags for Multiplex Immunophenotyping Cellular Receptors and Imaging Tumor Cells. *Small.* 2015;11:4149-57.
- [16] M. S. Strozyk, D. J. de Aberasturi, J. V. Gregory, M. Brust, J. Lahann, L. M. Liz-Marzán. Spatial Analysis of Metal-PLGA Hybrid Microstructures Using 3D SERS Imaging. *Adv. Funct. Mater.* 2017;27:1701626.
- [17] M. S. Strozyk, D. Jimenez de Aberasturi, L. M. Liz-Marzán. Composite Polymer Colloids for SERS-Based Applications. *Chem. Rec.* 2018;18:807-18.
- [18] C. Zong, M. Xu, L.-J. Xu, T. Wei, X. Ma, X.-S. Zheng, R. Hu, B. Ren. Surface-Enhanced Raman Spectroscopy for Bioanalysis: Reliability and Challenges. *Chem. Rev.* 2018;118:4946-80.
- [19] S. de Vitis, M. L. Coluccio, F. Gentile, N. Malara, G. Perozziello, E. Dattola, P. Candeloro, E. Di Fabrizio. Surface enhanced Raman spectroscopy measurements of MCF7 cells adhesion in confined micro-environments. *Opt. Lasers Eng.* 2016;76:9-16.
- [20] J. Wang, K. M. Koo, E. J. H. Wee, Y. Wang, M. Trau. A nanoplasmonic label-free surface-enhanced Raman scattering strategy for non-invasive cancer genetic subtyping in patient samples. *Nanoscale.* 2017;9:3496-503.
- [21] Y. Wang, S. Kang, A. Khan, G. Ruttner, S. Y. Leigh, M. Murray, S. Abeytunge, G. Peterson, M. Rajadhyaksha, S. Dintzis, S. Javid, J. T. C. Liu. Quantitative molecular phenotyping with topically applied SERS nanoparticles for intraoperative guidance of breast cancer lumpectomy. *Sci. Rep.* 2016;6:21242.
- [22] V. Moisoiu, A. Socaciu, A. Stefanu, S. Iancu, I. Boros, C. Alecsa, C. Rachieriu, A. Chiorean, D. Eniu, N. Leopold, C. Socaciu, D. Eniu. Breast Cancer Diagnosis by Surface-Enhanced Raman Scattering (SERS) of Urine. *Appl. Sci.* 2019;9:806.
- [23] Y.-F. Huang, H.-P. Zhu, G.-K. Liu, D.-Y. Wu, B. Ren, Z.-Q. Tian. When the signal is not from the original molecule to be detected: chemical transformation of para-aminothiophenol on Ag during the SERS

measurement. *J. Am. Chem. Soc.* 2010;132:9244-46.

[24] A. Shamsaie, M. Jonczyk, J. Sturgis, J. Paul Robinson, J. Irudayaraj. Intracellularly grown gold nanoparticles as potential surface-enhanced Raman scattering probes. *J. Biomed. Opt.* 2007;12:20502.

[25] C. D. Walkey, W. C. W. Chan. Understanding and controlling the interaction of nanomaterials with proteins in a physiological environment. *Chem. Soc. Rev.* 2012;41:2780-99.

[26] X.-S. Zheng, I. J. Jahn, K. Weber, D. Cialla-May, J. Popp. Label-free SERS in biological and biomedical applications: Recent progress, current challenges and opportunities. *Spectrochim. Acta A. Mol. Biomol. Spectrosc.* 2018;197:56-77.

[27] S. Laing, L. E. Jamieson, K. Faulds, D. Graham. Surface-enhanced Raman spectroscopy for in vivo biosensing. *Nat. Rev. Chem.* 2017;1:501.

[28] B. Pelaz, G. Charron, C. Pfeiffer, Y. Zhao, J. M. de La Fuente, X.-J. Liang, W. J. Parak, P. Del Pino. Interfacing engineered nanoparticles with biological systems: anticipating adverse nano-bio interactions. *Small.* 2013;9:1573-84.

[29] J. Piella, N. G. Bastús, V. Puentes. Size-Dependent Protein-Nanoparticle Interactions in Citrate-Stabilized Gold Nanoparticles: The Emergence of the Protein Corona. *Bioconjug. Chem.* 2017;28:88-97.

[30] N. M. S. Sirimuthu, C. D. Syme, J. M. Cooper. Investigation of the stability of labelled nanoparticles for SE(R)RS measurements in cells. *Chem. Commun.* 2011;47:4099-101.

[31] Arbeitsausschuss Chemische Terminologie (AChT) im DIN Deutsches Institut für Normung e.V. DIN 32645:2008-11, Chemische Analytik - Nachweis-, Erfassungs- und Bestimmungsgrenze unter Wiederholbedingungen - Begriffe, Verfahren, Auswertung, Beuth Verlag GmbH, Berlin. 2008.

[32] ICH Secretariat. ICH-Q2(R1) Validation of analytical procedures: Text and Methodology: International Conference on Harmonization (ICH) of Technical Requirements for the Registration of Pharmaceuticals for Human Use, Geneva. 2005.

[33] Z. Zhang, L. Wang, J. Wang, X. Jiang, X. Li, Z. Hu, Y. Ji, X. Wu, C. Chen. Mesoporous silica-coated gold nanorods as a light-mediated multifunctional theranostic platform for cancer treatment. *Adv. Mater.* 2012;24:1418-23.

[34] D. Rodríguez-Fernández, J. Langer, M. Henriksen-Lacey, L. M. Liz-Marzán. Hybrid Au–SiO₂ Core–Satellite Colloids as Switchable SERS Tags. *Chem. Mater.* 2015;27:2540-45.

[35] A. F. Stewart, A. Lee, A. Ahmed, S. Ip, E. Kumacheva, G. C. Walker. Rational design for the controlled aggregation of gold nanorods via phospholipid encapsulation for enhanced Raman scattering. *ACS Nano.* 2014;8:5462-667.

- [36] J. H. Kang, Y. T. Ko. Lipid-coated gold nanocomposites for enhanced cancer therapy. *Int. J. Nanomedicine*. 2015;10:33-45.
- [37] S. Y. Ip, C. M. MacLaughlin, N. Mullaithilaga, M. Joseph, S. Wala, C. Wang, G. C. Walker. Lipid-encapsulation of surface enhanced Raman scattering (SERS) nanoparticles and targeting to chronic lymphocytic leukemia (CLL) cells. *SPIE*. 2012;8212:821204.
- [38] U. S. Dinish, Z. Song, C. J. H. Ho, G. Balasundaram, A. B. E. Attia, X. Lu, B. Z. Tang, B. Liu, M. Olivo. Single Molecule with Dual Function on Nanogold: Biofunctionalized Construct for In Vivo Photoacoustic Imaging and SERS Biosensing. *Adv. Funct. Mater.* 2015;25:2316-25.
- [39] P. Verderio, S. Avvakumova, G. Alessio, M. Bellini, M. Colombo, E. Galbiati, S. Mazzucchelli, J. P. Avila, B. Santini, D. Prospero. Delivering colloidal nanoparticles to mammalian cells: a nano-bio interface perspective. *Adv. Healthc. Mater.* 2014;3:957-76.
- [40] Y. Wang, S. Schlücker. Rational design and synthesis of SERS labels. *Analyst*. 2013;138:2224-38.
- [41] Y. Wang, A. B. Serrano, K. Sentosun, S. Bals, L. M. Liz-Marzán. Stabilization and Encapsulation of Gold Nanostars Mediated by Dithiols. *Small*. 2015;11:4314-20.
- [42] B. Khlebtsov, T. Pylaev, V. Khanadeev, D. Bratashov, N. Khlebtsov. Quantitative and multiplex dot-immunoassay using gap-enhanced Raman tags. *RSC Adv*. 2017;7:40834-41.
- [43] H.-M. Kim, D.-M. Kim, C. Jeong, S. Y. Park, M. G. Cha, Y. Ha, D. Jang, S. Kyeong, X.-H. Pham, E. Hahm, S. H. Lee, D. H. Jeong, Y.-S. Lee, D.-E. Kim, B.-H. Jun. Assembly of Plasmonic and Magnetic Nanoparticles with Fluorescent Silica Shell Layer for Tri-functional SERS-Magnetic-Fluorescence Probes and Its Bioapplications. *Sci. Rep.* 2018;8:13938.
- [44] D. Zhu, Z. Wang, S. Zong, H. Chen, X. Wu, Y. Pei, P. Chen, X. Ma, Y. Cui. Ag@4ATP-coated liposomes: SERS traceable delivery vehicles for living cells. *Nanoscale*. 2014;6:8155-61.
- [45] G. von White, Y. Chen, J. Roder-Hanna, G. D. Bothun, C. L. Kitchens. Ag@4ATP-coated liposomes: SERS traceable delivery vehicles for living cells. *ACS Nano*. 2012;6:4678-85.
- [46] H.-Y. Lee, S. H. R. Shin, L. L. Abezgauz, S. A. Lewis, A. M. Chirsan, D. D. Danino, K. J. M. Bishop. Integration of gold nanoparticles into bilayer structures via adaptive surface chemistry. *J. Am. Chem. Soc.* 2013;135:5950-53.
- [47] J. Nam, Y. S. Ha, S. Hwang, W. Lee, J. Song, J. Yoo, S. Kim. pH-responsive gold nanoparticles-in-liposome hybrid nanostructures for enhanced systemic tumor delivery. *Nanoscale*. 2013;5:10175-78.
- [48] T. Lajunen, L. Viitala, L.-S. Kontturi, T. Laaksonen, H. Liang, E. Vuorimaa-Laukkanen, T. Viitala, X. Le Guével, M. Yliperttula, L. Murtomäki, A. Urtti. Light induced cytosolic drug delivery from liposomes with gold nanoparticles. *J. Control. Release*. 2015;203:85-98.

- [49] B. Y. Moghadam, W.-C. Hou, C. Corredor, P. Westerhoff, J. D. Posner. Role of nanoparticle surface functionality in the disruption of model cell membranes. *Langmuir*. 2012;28:16318-26.
- [50] E. M. Curtis, A. H. Bahrami, T. R. Weikl, C. K. Hall. Modeling nanoparticle wrapping or translocation in bilayer membranes. *Nanoscale*. 2015;7:14505-14.
- [51] D. Ag Seleci, V. Maurer, F. B. Barlas, J. C. Porsiel, B. Temel, E. Ceylan, S. Timur, F. Stahl, T. Scheper, G. Garnweitner. Transferrin-Decorated Niosomes with Integrated InP/ZnS Quantum Dots and Magnetic Iron Oxide Nanoparticles: Dual Targeting and Imaging of Glioma. *Int. J. Mol. Sci*. 2021;22:4556.
- [52] D. Ag Seleci, M. Seleci, J.-G. Walter, F. Stahl, T. Scheper. Niosomes as Nanoparticulate Drug Carriers: Fundamentals and Recent Applications. *J. Nanomater*. 2016;2016:7372306.
- [53] D. Ag Seleci, V. Maurer, F. Stahl, T. Scheper, G. Garnweitner. Rapid Microfluidic Preparation of Niosomes for Targeted Drug Delivery. *Int. J. Mol. Sci*. 2019;20:4696.
- [54] Shilpa, B. P. Srinivasan, M. Chauhan. Niosomes as vesicular carriers for delivery of proteins and biologicals. *Int. J. Drug. Del*. 2011;3:14-24.
- [55] S. Moghassemi, A. Hadjizadeh. Nano-niosomes as nanoscale drug delivery systems: an illustrated review. *J. Control. Release*. 2014;185:22-36.
- [56] C. Marianecchi, L. Di Marzio, F. Rinaldi, C. Celia, D. Paolino, F. Alhaique, S. Esposito, M. Carafa. Niosomes from 80s to present: the state of the art. *Adv. Colloid. Interface. Sci*. 2014;205:187-206.
- [57] I. F. Uchegbu, S. P. Vyas. Non-ionic surfactant based vesicles (niosomes) in drug delivery. *Int. J. Pharm*. 1998;172:33-70.
- [58] D. Ag Seleci, M. Seleci, F. Stahl, T. Scheper. Tumor homing and penetrating peptide-conjugated niosomes as multi-drug carriers for tumor-targeted drug delivery. *RSC Adv*. 2017;7:33378-84.
- [59] M. G. Arafa, D. Ghalwash, D. M. El-Kersh, M. M. Elmazar. Propolis-based niosomes as oromuco-adhesive films: A randomized clinical trial of a therapeutic drug delivery platform for the treatment of oral recurrent aphthous ulcers. *Sci. Rep*. 2018;8:18056.
- [60] I. P. Kaur, D. Aggarwal, H. Singh, S. Kakkar. Improved ocular absorption kinetics of timolol maleate loaded into a bioadhesive niosomal delivery system. *Graefes Arch. Clin. Exp. Ophthalmol*. 2010;248:1467-72.
- [61] L. Seguella, F. Rinaldi, C. Marianecchi, R. Capuano, M. Pesce, G. Annunziata, F. Casano, G. Bassotti, A. Sidoni, M. Milone, G. Aprea, G. D. de Palma, M. Carafa, M. Pesce, G. Esposito, G. Sarnelli. Pentamidine niosomes thwart S100B effects in human colon carcinoma biopsies favouring wtp53 rescue. *J. Cell Mol. Med*. 2020;24:3053-63.

- [62] V. Maurer, C. Frank, J. C. Porsiel, S. Zellmer, G. Garnweitner, R. Stosch. Step-by-step monitoring of a magnetic and SERS-active immunosensor assembly for purification and detection of tau protein. *J. Biophotonics*. 2020;13:e201960090.
- [63] V. Maurer, S. Altin, D. Ag Seleci, A. Zarinwall, B. Temel, P. M. Vogt, S. Strauß, F. Stahl, T. Scheper, V. Bucan, G. Garnweitner. In-Vitro Application of Magnetic Hybrid Niosomes: Targeted siRNA-Delivery for Enhanced Breast Cancer Therapy. *Pharmaceutics*. 2021;13:394.
- [64] S. Jose, C. T. A, R. Sebastian, S. M. H, A. N. A, A. Durazzo, M. Lucarini, A. Santini, E. B. Souto. Transferrin-Conjugated Docetaxel-PLGA Nanoparticles for Tumor Targeting: Influence on MCF-7 Cell Cycle. *Polymers*. 2019;11:1905.
- [65] H. A. Joshi, E. S. Attar, P. Dandekar, P. V. Devarajan, Transferrin Receptor and Targeting Strategies. in *Targeted Intracellular Drug Delivery by Receptor Mediated Endocytosis*, Vol. 39, AAPS Advances in the Pharmaceutical Sciences Series (Eds: P. V. Devarajan, P. Dandekar, A. A. D'Souza), Springer International Publishing, Cham. 2019:457-80.
- [66] D. S. Grubisha, R. J. Lipert, H.-Y. Park, J. Driskell, M. D. Porter. Femtomolar detection of prostate-specific antigen: an immunoassay based on surface-enhanced Raman scattering and immunogold labels. *Anal. Chem*. 2003;75:5936-43.
- [67] D. Zhu, Z. Wang, S. Zong, Y. Zhang, C. Chen, R. Zhang, B. Yun, Y. Cui. Investigating the Intracellular Behaviors of Liposomal Nanohybrids via SERS: Insights into the Influence of Metal Nanoparticles. *Theranostics*. 2018;8:941-54.
- [68] C. Kojima, Y. Hirano, E. Yuba, A. Harada, K. Kono. Preparation and characterization of complexes of liposomes with gold nanoparticles. *Colloids Surf. B Biointerfaces*. 2008;66:246-52.
- [69] J. Rejman, V. Oberle, I. S. Zuhorn, D. Hoekstra. Size-dependent internalization of particles via the pathways of clathrin- and caveolae-mediated endocytosis. *Biochem. J*. 2004;377:159-69.
- [70] D. Drescher, J. Kneipp. Nanomaterials in complex biological systems: insights from Raman spectroscopy. *Chem. Soc. Rev*. 2012;41:5780-99.
- [71] H. Hillaireau, P. Couvreur, Cell. Nanocarriers' entry into the cell: relevance to drug delivery. *Mol. Life Sci*. 2009;66:2873-96.
- [72] Y. Shen, X. Li, D. Dong, B. Zhang, Y. Xue, P. Shang. Transferrin receptor 1 in cancer: a new sight for cancer therapy. *Am. J. Cancer Res*. 2018;8:916-31.
- [73] S. Pizzamiglio, M. de Bortoli, E. Taverna, M. Signore, S. Veneroni, W. C.-S. Cho, R. Orlandi, P. Verderio, I. Bongarzone. Expression of Iron-Related Proteins Differentiate Non-Cancerous and Cancerous Breast Tumors. *Int. J. Mol. Sci*. 2017;18.

- [74] H. O. Habashy, D. G. Powe, C. M. Staka, E. A. Rakha, G. Ball, A. R. Green, M. Aleskandarany, E. C. Paish, R. Douglas Macmillan, R. I. Nicholson, I. O. Ellis, J. M. W. Gee. Transferrin receptor (CD71) is a marker of poor prognosis in breast cancer and can predict response to tamoxifen. *Breast Cancer Res. Treat.* 2010;119:283-93.
- [75] W. Wang, Z. Deng, H. Hatcher, L. D. Miller, X. Di, L. Tesfay, G. Sui, R. B. D'Agostino, F. M. Torti, S. V. Torti. IRP2 regulates breast tumor growth. *Cancer Res.* 2014;74:497-507.
- [76] A. Zarinwall, M. Asadian-Birjand, D. A. Seleci, V. Maurer, A. Trautner, G. Garnweitner, H. Fuchs. Magnetic Nanoparticle-Based Dianthin Targeting for Controlled Drug Release Using the Endosomal Escape Enhancer SO1861. *Nanomaterials.* 2021;11:1057.
- [77] M. Nag, V. Gajbhiye, P. Kesharwani, N. K. Jain. Transferrin functionalized chitosan-PEG nanoparticles for targeted delivery of paclitaxel to cancer cells. *Colloids Surf. B Biointerfaces.* 2016;148:363-70.
- [78] S. Zakel, S. Wundrack, G. O'Connor, B. Güttler, R. Stosch. Validation of isotope dilution surface-enhanced Raman scattering (IDSERS) as a higher order reference method for clinical measurands employing international comparison schemes. *J. Raman Spectrosc.* 2013;44:1246-52.
- [79] C. Frank, C. Brauckmann, M. Palos, C. G. Arsene, J. Neukammer, M. E. Del Castillo Busto, S. Zakel, C. Swart, B. Güttler, R. Stosch. Comparison of potential higher order reference methods for total haemoglobin quantification-an interlaboratory study. *Anal. Bioanal. Chem.* 2017;409:2341-51.
- [80] C. Frank, O. Rienitz, R. Jährling, D. Schiel, S. Zakel. Reference measurement procedures for the iron saturation in human transferrin based on IDMS and Raman scattering. *Metallomics.* 2012;4:1239-44.
- [81] A. F. Oskooi, D. Roundy, M. Ibanescu, P. Bermel, J. D. Joannopoulos, S. G. Johnson. Meep: A flexible free-software package for electromagnetic simulations by the FDTD method. *Comput. Phys. Commun.* 2010;181:687-702.
- [82] C. V. Yerin, V. I. Lykhmanova, M. V. Yerina. Spectral dependences of the complex refractive index of concentrated magnetic fluids. *Magnetohydrodynamics.* 2018;54:157-62.
- [83] P. B. Johnson, R. W. Christy. Optical Constants of the Noble Metals. *Phys. Rev. B* 1972;6:4370-79.
- [84] S. Saavedra-Alonso, P. Zapata-Benavides, A. K. Chavez-Escamilla, E. Manilla-Muñoz, D. E. Zamora-Avila, M. A. Franco-Molina, C. Rodriguez-Padilla. WT1 shRNA delivery using transferrin-conjugated PEG liposomes in an in vivo model of melanoma. *Exp. Ther. Med.* 2016;12:3778-84.
- [85] American Society for Testing and Materials. E1840-96, Standard guide for raman shift standards for spectrometer calibration. 2007.

Figures

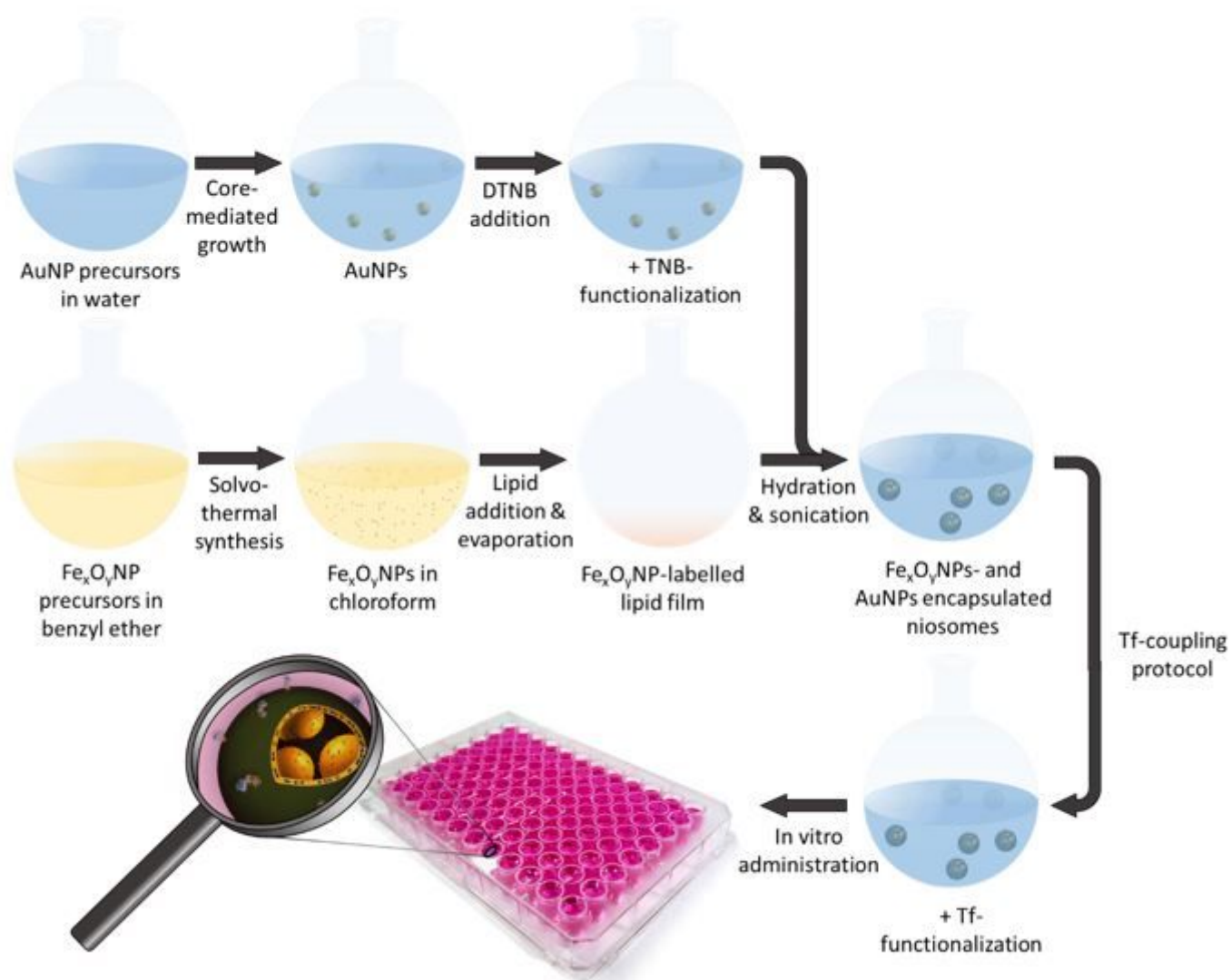


Figure 1

Schematic depiction of the AuNPs/Fe_xO_yNPs/NIO/Tf formation and application.

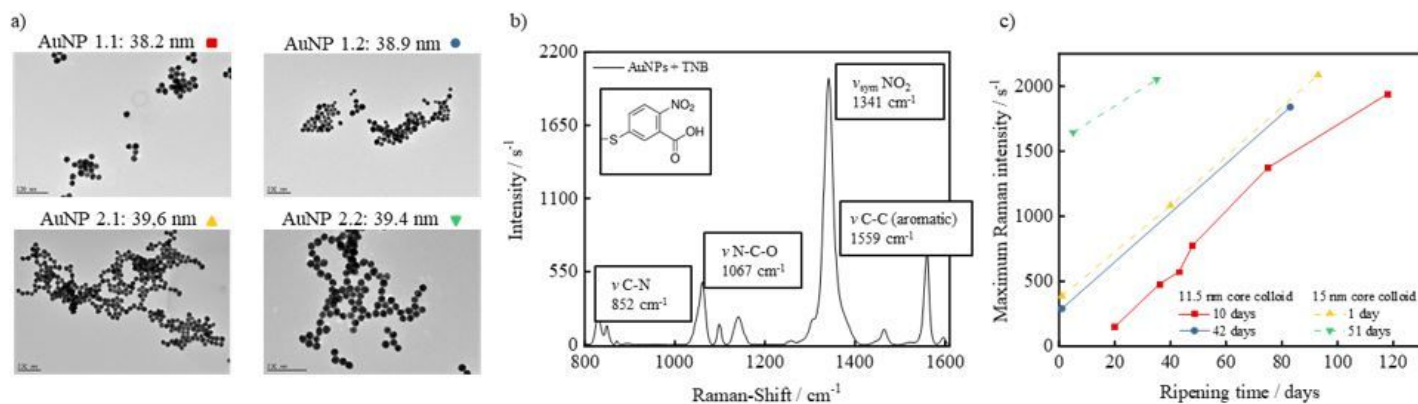


Figure 2

a) Representative TEM images of the four ascorbate-stabilized AuNPs samples; b) SERS spectrum with four characteristic vibrational assignments of TNB-functionalized AuNPs and c) maximum Raman intensity (= intensity of the nitric group stretch) measured throughout the ripening time of the four AuNP solutions shown in a), which were synthesized using differently sized core colloids (11.5 nm and 15.0 nm) after respective core colloid ripening times (10 and 42 days as well as 1 and 51 days).

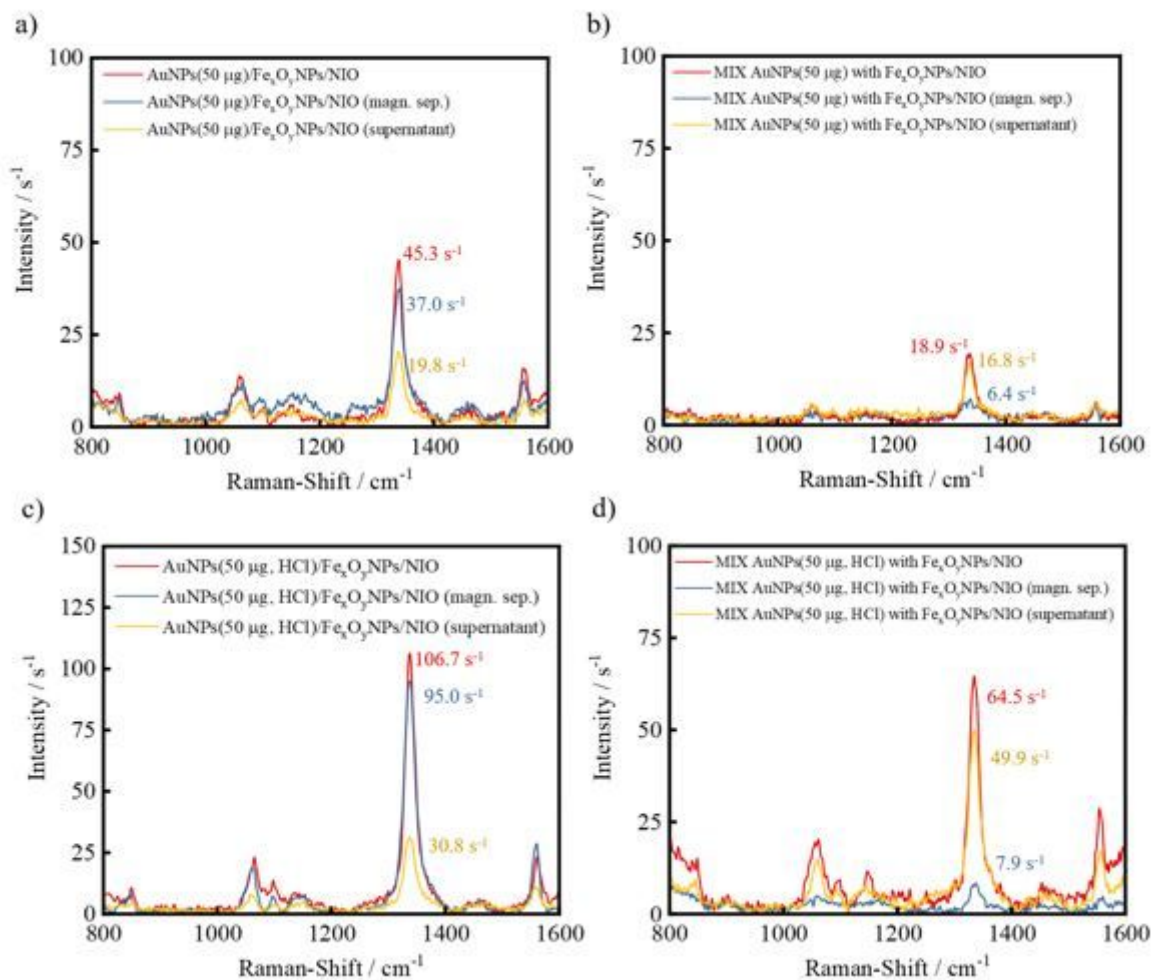


Figure 3

SERS spectra measured before and after magnetic separation obtained from the a) hybrid niosomes, b) negative control, c) hybrid niosomes with previously added HCl and d) negative control with previously added HCl.

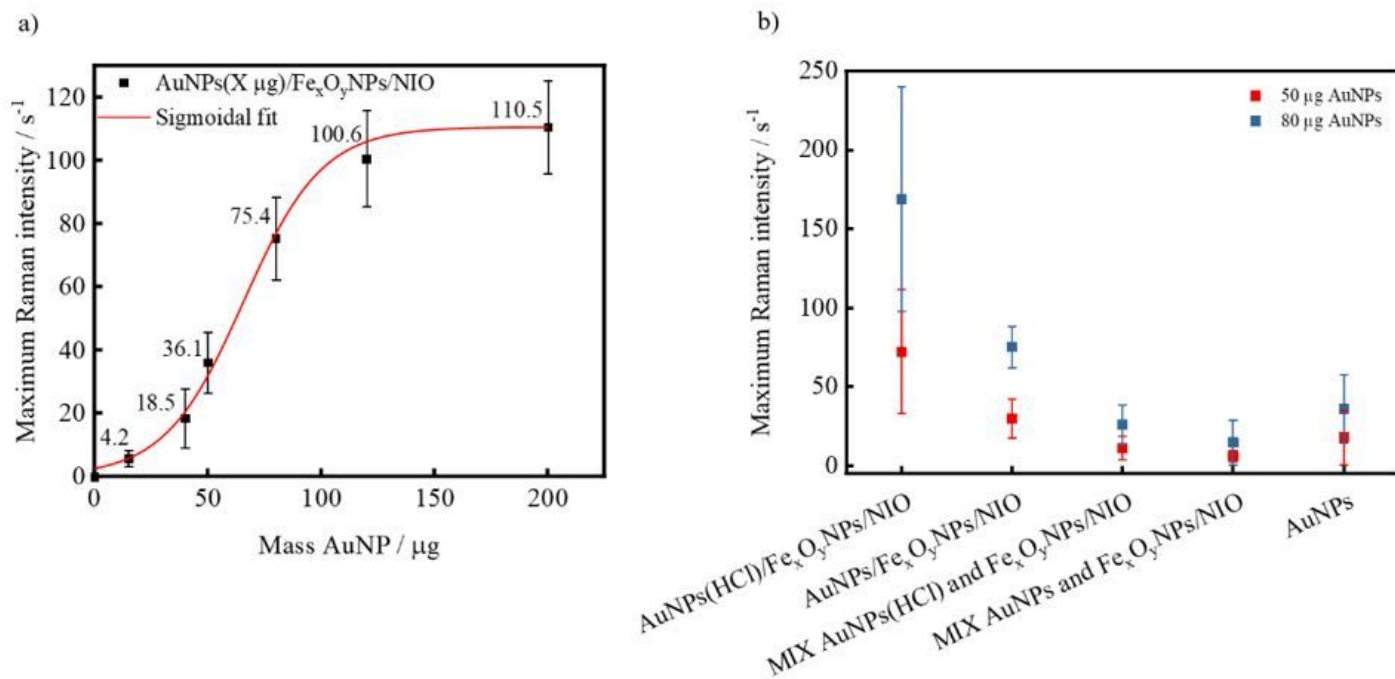


Figure 4

Measured maximum Raman intensities of a) hybrid niosomes after addition of different AuNP mass fractions and b) hybrid niosomes and negative controls (with a utilized AuNP mass of both 50 μg and 80 μg) in dependence of a previous HCl addition.

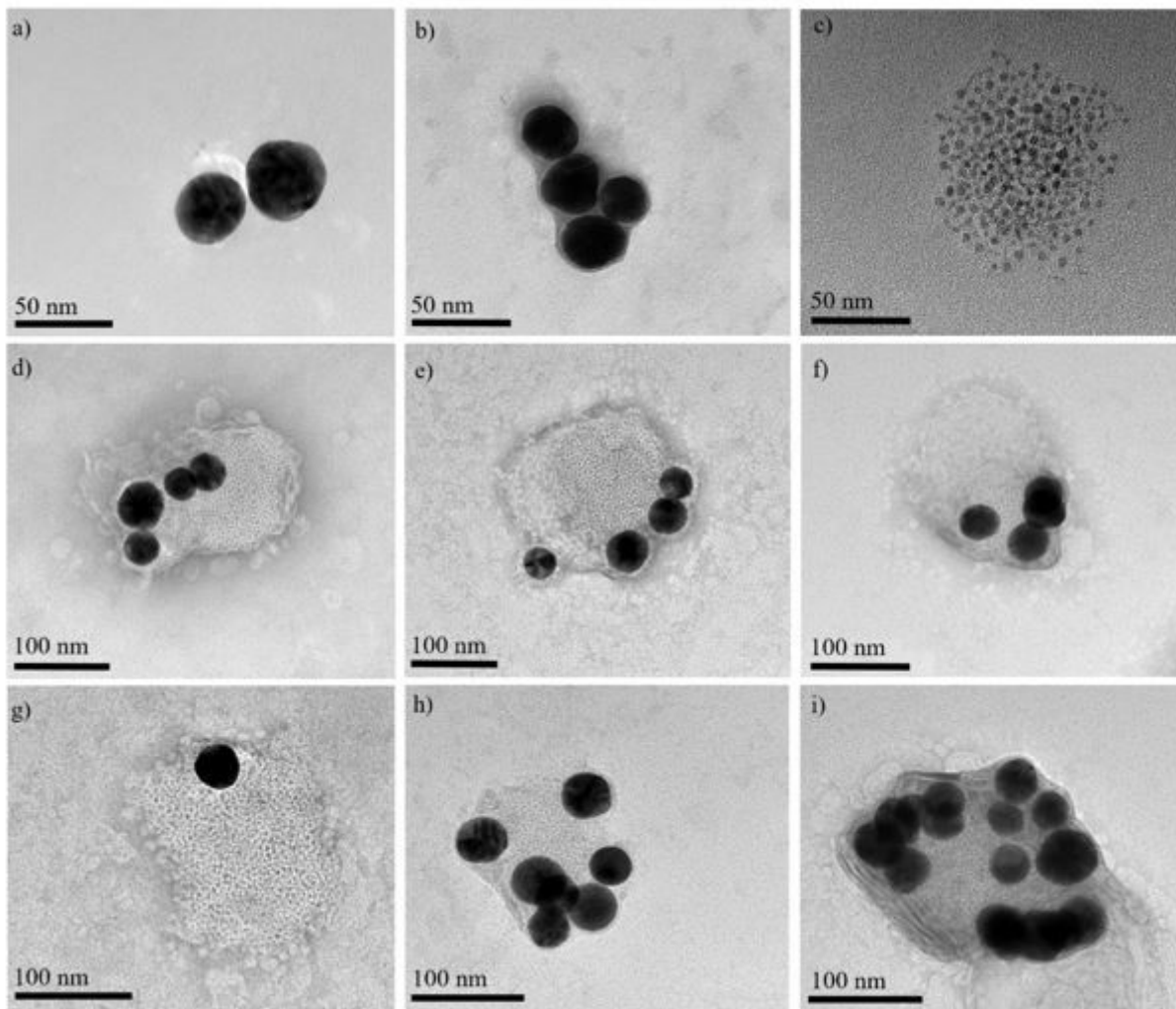


Figure 5

Representative TEM images of a) TNB-functionalized AuNPs, b) AuNP-loaded niosomes, c) FexOyNPs/NIO, d)-i) AuNPs/FexOyNPs/NIO hybrid niosomes.

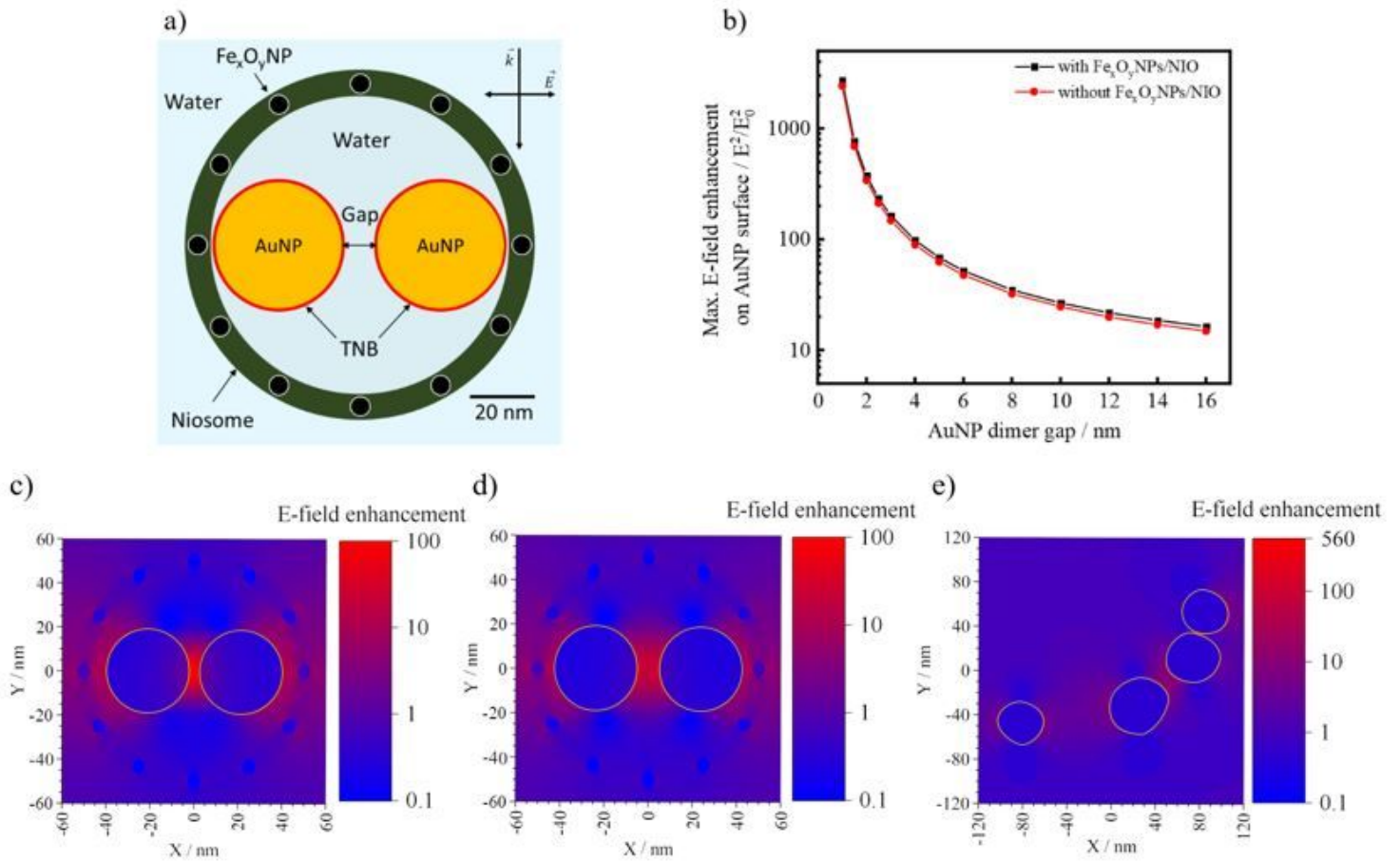


Figure 6

a) Schematic representation of AuNPs/Fe_xO_yNPs/NIO utilized for the FDTD simulations; b) calculated maximum E-field enhancement on the AuNP surface for AuNPs/Fe_xO_yNPs/NIO and AuNPs/NIO with variant interparticle gap; FDTD simulated E-field enhancement of AuNPs/Fe_xO_yNPs/NIO with a AuNP (encircled in gold) gap distance of 4 nm c), 10 nm d) and the AuNPs/Fe_xO_yNPs/NIO from the Figure 5 e) TEM image.

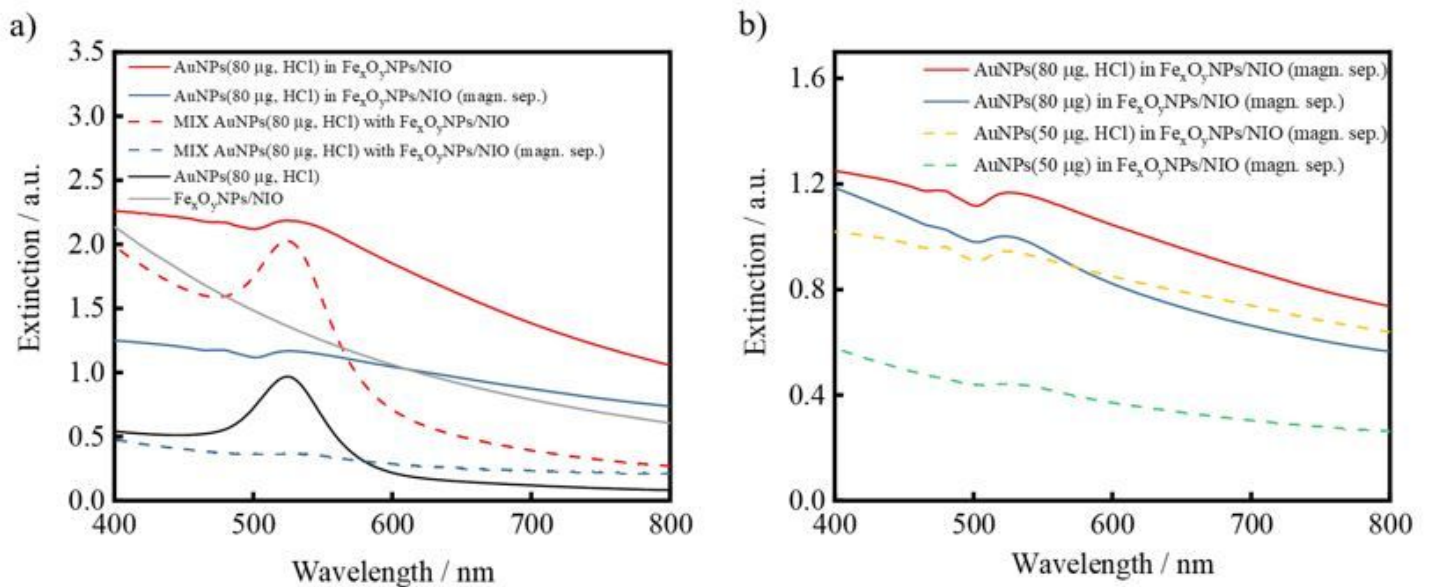


Figure 7

Measured UV/Vis spectra a) before and after magnetic purification obtained from hybrid niosomes and negative controls and b) hybrid niosomes with different AuNPs mass fractions as well as with and without previously added HCl.

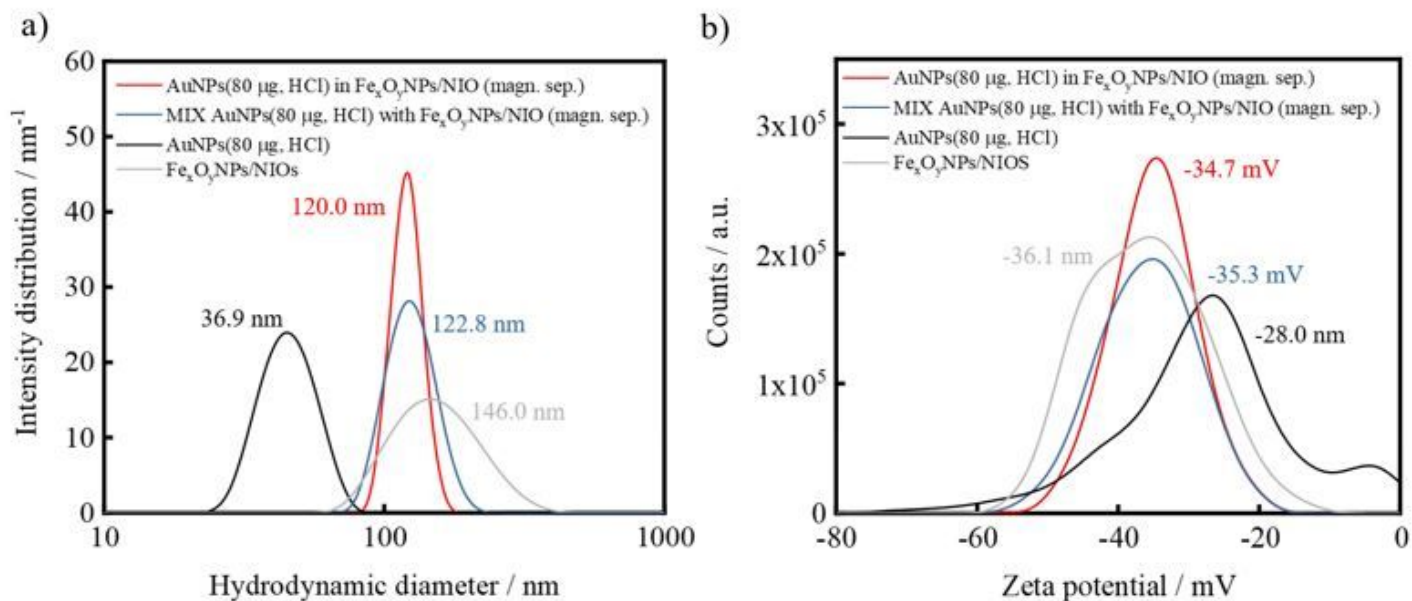


Figure 8

a) DLS measurements and b) Zeta potentials of the hybrid niosomes and negative control.

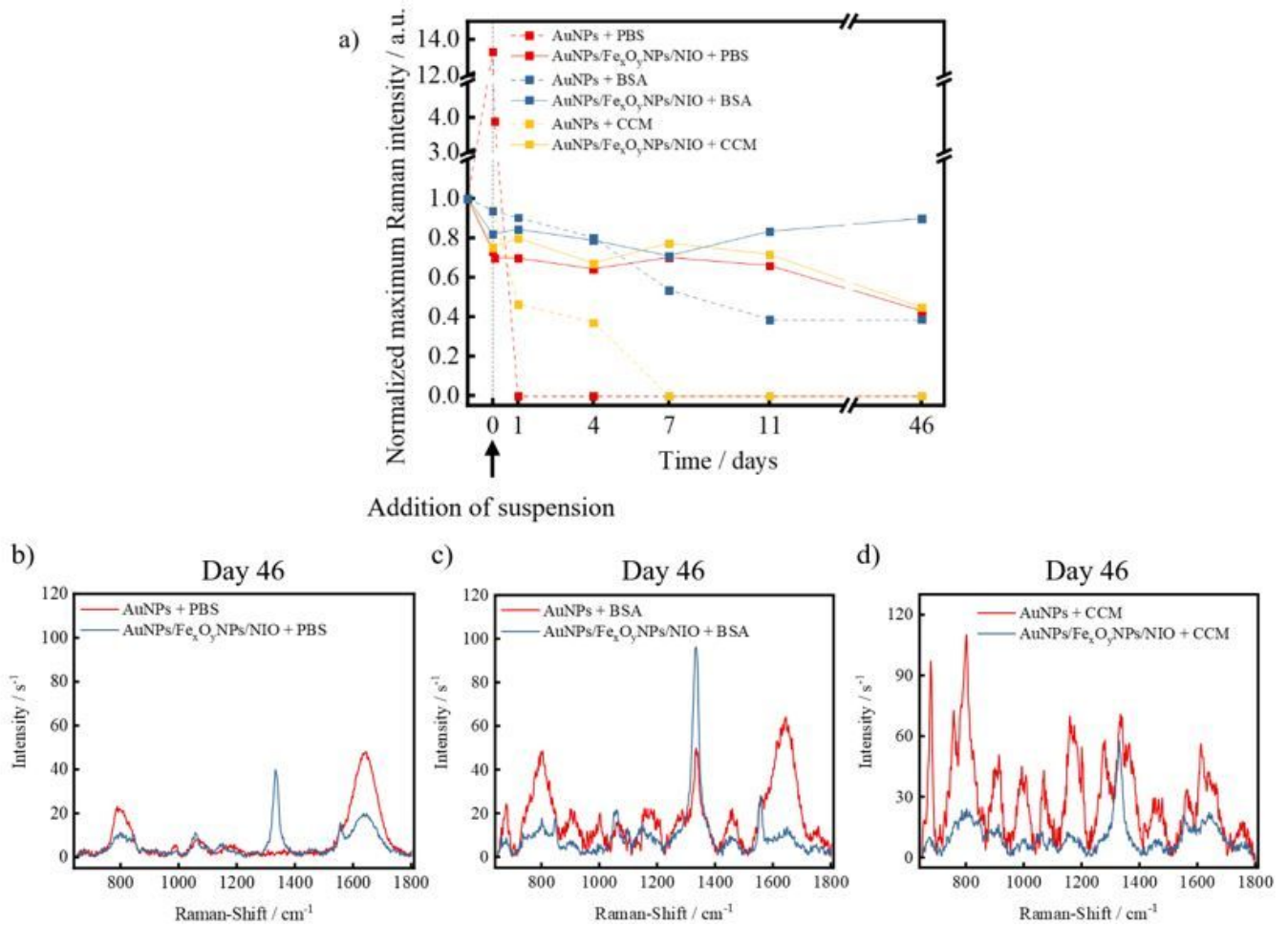


Figure 9

a) SERS-signal intensity variations of AuNPs/Fe₃O₄NPs/NIO and plain TNB-functionalized AuNPs throughout 46 days after addition of the respective medium (PBS, BSA or CCM); b-d) SERS-spectra of the hybrid niosomes and plain TNB-functionalized AuNPs on the 46th day after addition of PBS, BSA and CCM.

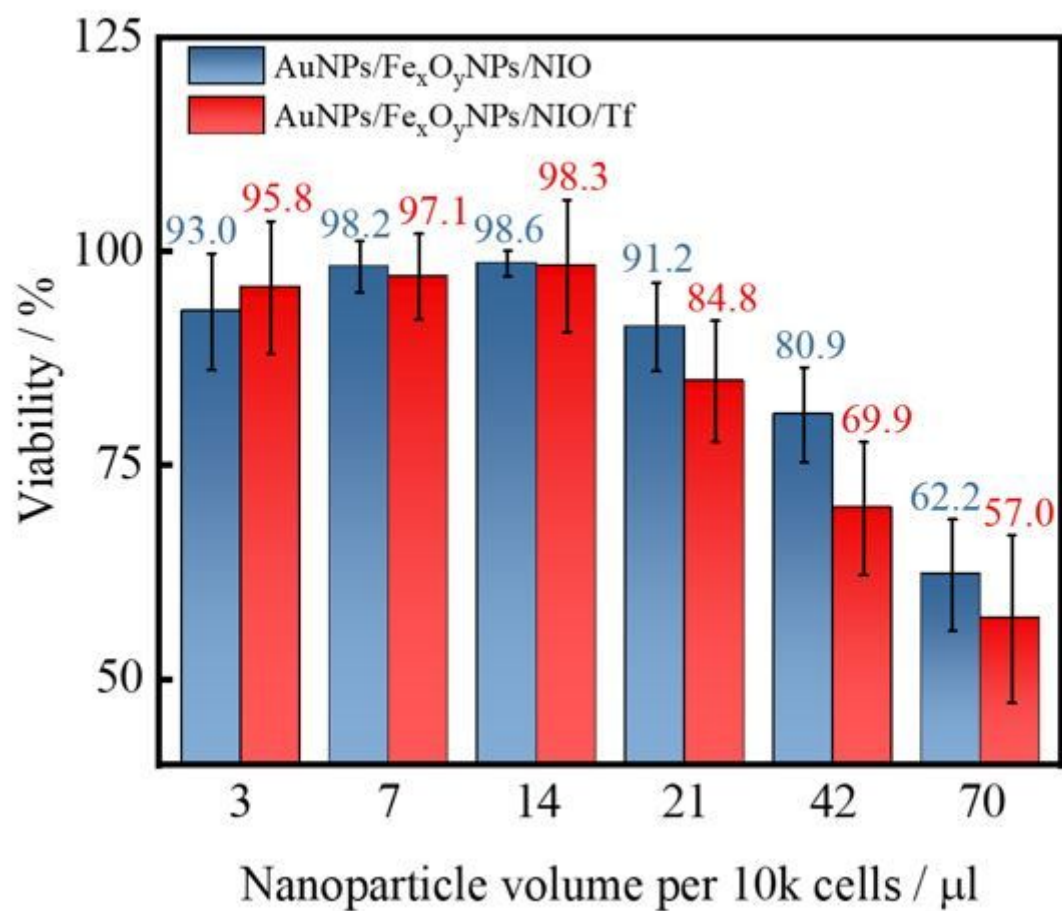


Figure 10

Viability of MCF-7 cells after in vitro administration of hybrid niosomes with or without Tf-functionalization and incubation under influence of an external magnetic field.

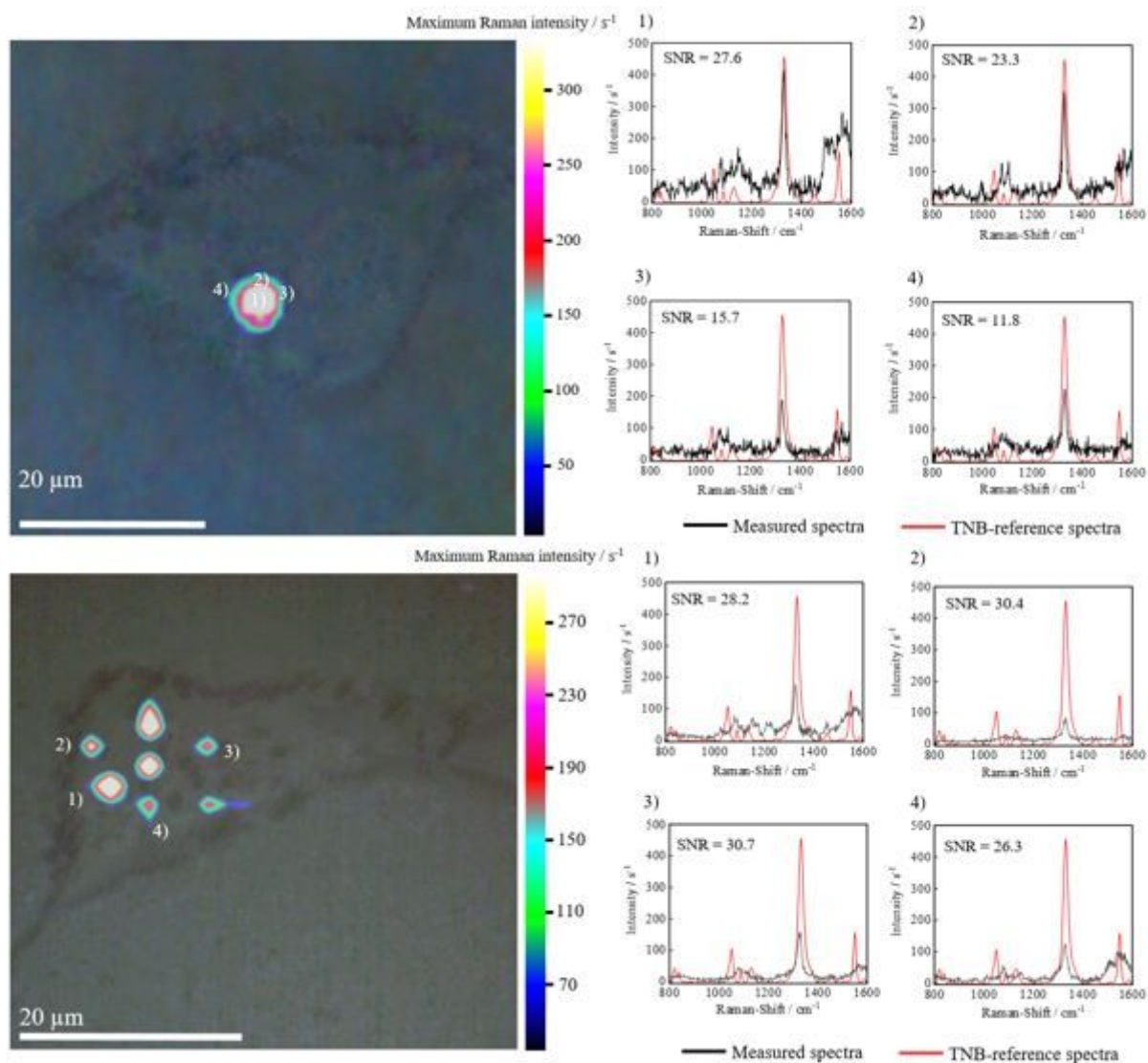


Figure 11

(left) Merged bright field and 2D-SERS mapping images of MCF-7 cells incubated with AuNPs/FexOyNPs/NIO with the scale bars showing the maximum Raman intensities, (right) SERS-spectra and the respective signal-to-noise ratios (SNR) of the displayed 2D-SERS signals.

Supplementary Files

This is a list of supplementary files associated with this preprint. Click to download.

- [Additionalfile1.docx](#)